

ヒト上顎大臼歯部欠損形態の違いにおける

顎骨構造の放射線・組織学的研究

神垣友希乃

The radiological and histological study on the human maxillary morphology
according to the difference by tooth-missing condition

Yukino
KAMIGAKI

日本歯科大学大学院生命歯学研究科歯科臨床系専攻
(指導：代居 敬教授)

The Nippon Dental University
Graduate School of Life Dentistry at Tokyo
(Director : Prof. Takashi YOSUE)

(2017 年 1 月)

和文表題【ヒト上顎大臼歯部欠損形態の違いにおける 顎骨構造の放射線・組織学的研究】

和文著者氏名【神垣友希乃】

英文表題【The radiological and histological study on the human maxilla bone according to the type of missing of teeth】

英文著者氏名【Yukino KAMIGAKI】

緒 言

顎骨は歯を喪失すると、高さや幅の減少、その内部構造も大きく変化する^{1~4)}。この変化は歯科治療、とくにインプラント治療において大きく影響すると考えられる。骨の構造の分析は、骨密度や骨梁幅、骨梁数や骨梁構造などのさまざまな指標が存在する^{5~16)}。上顎については、骨の高さや幅の報告^{17~20)}がある。

第一大臼歯を喪失すると、中間歯欠損、遊離端欠損、無歯顎の3つの欠損形態に分類される。中間歯欠損は遊離端欠損よりも歯科治療に有利であるという報告^{17, 21)}や、上顎前歯部と臼歯部の骨質や骨密度の違いを示した報告^{11, 16, 22)}、骨の構造や組織学的観察の無歯顎における報告^{23~25)}はあるが、いずれも3つの欠損形態での放射線学的、また組織学的な比較検討はされていない。そこで本研究では、有歯顎と基準とし、中間歯欠損、遊離端欠損、無歯顎の3つの欠損形態別に、放射線・組織学的に上顎大臼歯部顎骨の骨質および骨梁の違いを検討した。

対象と方法

日本歯科大学解剖学第1講座から供与を受けた献体91体の左右171側の上顎第一大臼歯相当部を対象とした。内訳は男性46体の85側(59~93歳・平均 78.8 ± 8.29 歳)、女性45体の86側(61~103歳・平均 85.6 ± 8.77 歳)であった。欠損形態別の分類は有歯顎(男性17側・女性17側)、中間歯欠損(男性11側・女性6側)、遊離端欠損(男性26側・女性22側)、無歯顎(男性31側・女性41側)の4タイプに分け、歯科用コーンビームCT(CBCT)による分析、組織学的観察を行った。対象としたものは、Mischの基準²⁶⁾を参考に、高さ5 mm以上、幅6 mm以上、近遠心径7 mm以上を条件として選択した。

1. CBCT による撮影

上述した対象において、正中矢状面、フランクフルト平面を基準とし、撮影範囲は直径 79mm×80mm、ボクセルサイズ 0.155×0.155×0.155 mm にて 85 kV 4 mA、200 mg/cm³ ハイドロキシアパタイト参照体と共に CBCT (AZ 3000CT ; 朝日レントゲン) 撮影を行った。その後 NEOPREMIUM (朝日レントゲン) にて、矢状断は正中矢状面、水平断は口蓋平面、前頭断は有歯顎では第一大臼歯と第二大臼歯の間、中間歯欠損、遊離端欠損、無歯顎では頬骨下稜を基準とした断層像を得た (図 1)。

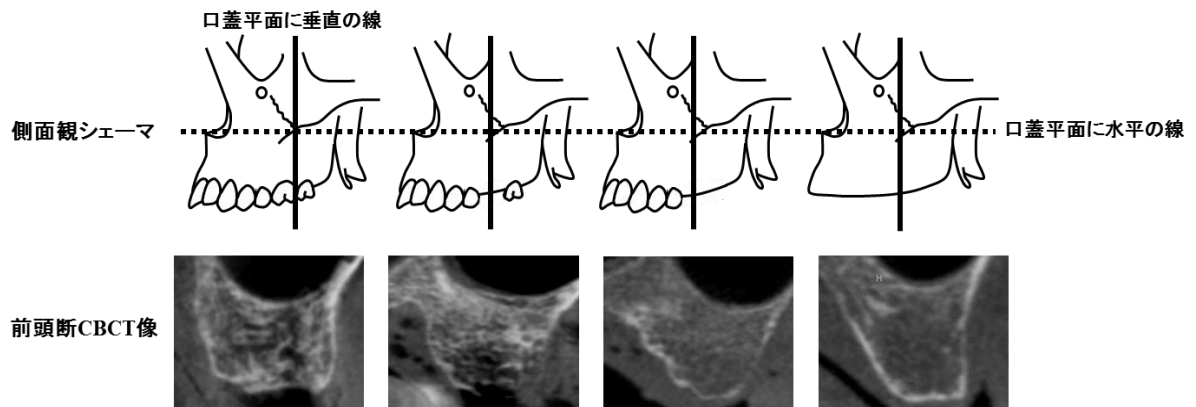


図 1 欠損形態別の側方観シェーマと前頭断 CBCT 像

NEOPREMIUM にて、口蓋平面に水平、正中矢状面にて矢状断した側面観から前頭断 CBCT 像を得た。前頭断の前後的基準は有歯顎では第一大臼歯と第二大臼歯の間、中間歯欠損、遊離端欠損、無歯顎では頬骨下稜における口蓋平面に垂直の線とした。前頭断 CBCT 像の代表例の献体の性別と年齢は、左から有歯顎男性 80 歳、中間歯欠損男性 80 歳、遊離端欠損女性 79 歳、無歯顎女性 97 歳である。

2. 骨構造の計測

得られた画像より、上顎洞底の最下部から歯槽突起の最上部を歯槽骨の高さ、上顎洞粘膜側の皮質骨の厚さ (上顎洞底の最下部から測定)、口腔粘膜側の皮質骨の厚さ (歯槽突起の最上部から測定) し、ImageJ 1.48 (U. S. National Institutes of Health) を用いて計測を行った (図 2)。

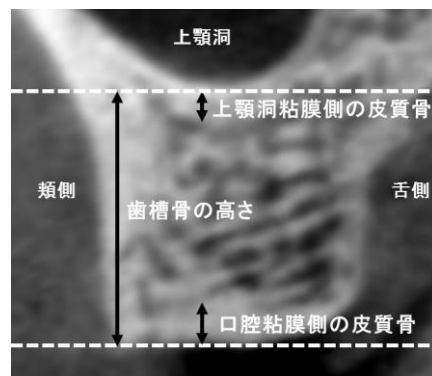


図2 骨構造の計測部位

歯槽骨の高さは上顎洞底最下部から歯槽突起の最上部までの距離とし、さらに上顎洞底の最下部から上顎洞粘膜側の皮質骨の厚さ、および歯槽突起の最上部から口腔粘膜側の皮質骨の厚さを計測した。

3. 骨梁構造の評価

骨梁構造の評価はCBCT所見より Lekholm & Zarb 分類（以下 LZ 分類）²⁷⁾ に準じて、薄い皮質骨に囲まれた骨の密度の高い海綿骨を S1（LZ 分類 Type 3）、薄い皮質骨に囲まれた骨の密度の低い海綿骨を S2（LZ 分類 Type 4）、不十分な骨構造や大きな空洞があるものを S3（LZ 分類該当するものなし）に分類をした（図3）。

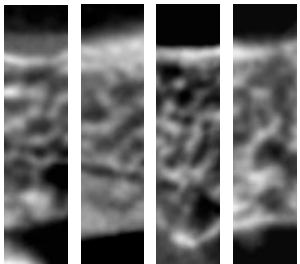
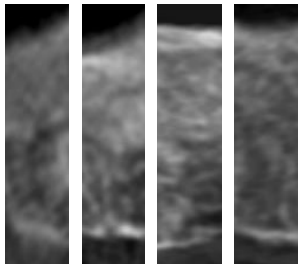
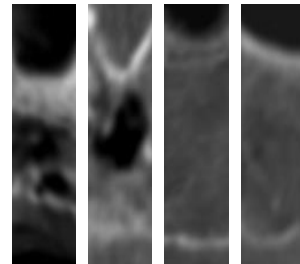
S 1	S 2	S 3
骨梁構造が密	骨梁構造が弱い	不十分な骨梁構造 大きな空洞があるもの
		

図3 骨梁構造の分類

S1 は骨梁構造が密なもので、代表例の献体の性別と年齢は、左から有歯顎女性 73 歳、男性 72 歳、男性 64 歳、男性 80 歳である。S2 は骨梁構造が弱いもので、左から遊離端欠損男性 77 歳、無歯顎男性 78 歳、男性 84 歳、男性 73 歳である。S3 は不十分な骨梁構造や

大きな空洞があるもので、左から遊離端欠損女性 89 歳、無歯顎女性 86 歳、女性 96 歳、男性 92 歳であった。

4. 骨密度の評価

海綿骨領域に対し、ImageJ 1.48 を用いてハイドロキシアパタイト参照体を基準として 2 値化した画像で骨密度の評価を行った（図 4）。

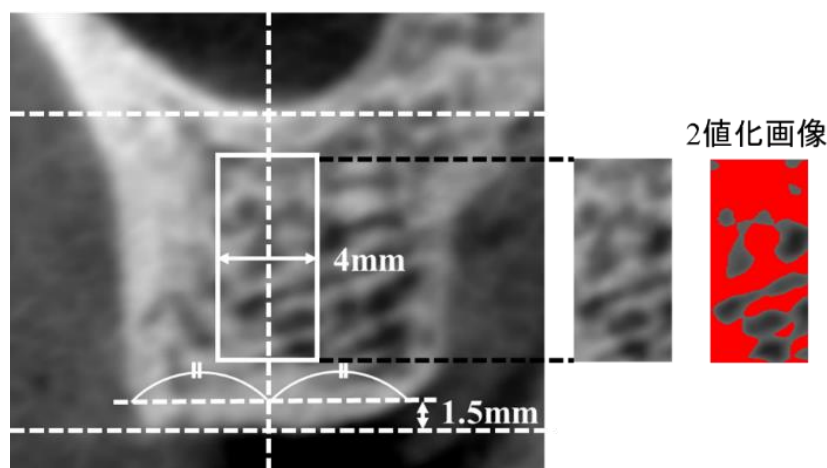


図 4 骨密度の評価部位

骨密度の評価方法は、歯槽突起の最上部に水平な線を基準として、1.5mm 歯槽部皮質骨に水平線を加え、これに対して直角に上顎洞底部と歯槽突起を結んだ線を垂直線とし、左右それぞれ 2mm ずつ計 4mm を水平幅とし、上下では上方を上顎洞側皮質骨の最下点で下方は歯槽部皮質骨までのボックス型を作図した。このボックス内の骨密度は、200 mg/cm³ ハイドロキシアパタイト参照体を基準として 2 値化して画像補正して解析を行った。

5. 組織学的観察

さらに無作為に抽出した有歯顎、中間歯欠損、遊離端欠損、無歯顎のそれぞれ 16 献体（平均年齢 80.4±7.61 歳）を対象に、垂直的に上顎骨を切断して PBS で洗浄後、4℃にて 21～36 日かけて 10%EDTA-PBS 溶液にて脱灰した。さらに PBS にて洗浄し、通法に従ってパラフィン包埋をした後、8 μm 厚の薄切切片を作製し染色を行った。この切片をアルコール・キシレン系列で脱パラフィン、PBS で洗浄後、内在性ペルオキシダーゼを 0.3% H₂O₂ 溶液で失活させた。G-Block（Genostaff Co., Ltd.）と Avidin/Biotin Blocking Kit（Vector

SP-2001, Vector Laboratory) によりブロッッキングを行った後、抗 CD31 抗体 (1:500, Lab Vision Corp, #RB-10333) を 4℃で一晩反応させた。コントロールには rabbit immunoglobulin fraction (Dako X0936) を用いた。TBS 洗浄後、二次抗体反応として biotin-conjugated goat anti-rabbit immunoglobulin (Dako) にて反応させ、peroxidase-conjugated streptavidin (Nichirei) を加え、ジアミノベンチジンにて発色を行った。Mayer's hematoxylin (Muto)により対比染色を行い、malinol (Muto) により封入した。組織切片は顕微鏡下 (DM-2500, Leica Microsystems) で上顎洞粘膜側から口腔粘膜側にかけて CBCT による計測と同部位の観察を行った (図 5)。

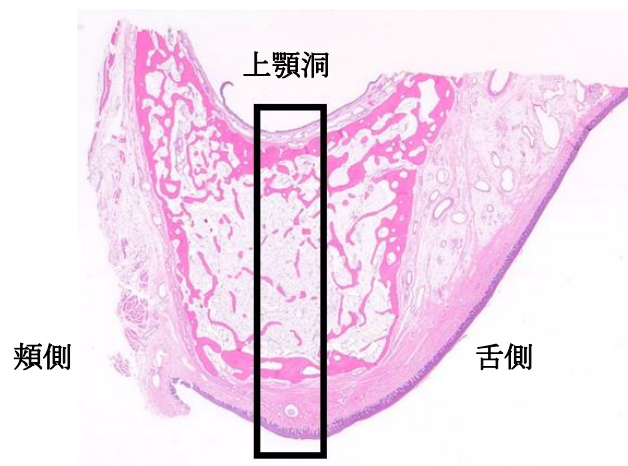


図 5 組織学的所見の観察部位

CBCT 画像の計測方法に対応した切片を作成して組織学的観察をおこなった。方法は CBCT 解析と同様に、歯槽突起の最上部に水平な線を基準として、1.5mm 歯槽部皮質骨に水平線を加え、これに対して直角に上顎洞底部と歯槽突起を結んだ線を垂直線とし、左右それぞれ 2mm ずつ計 4mm を水平幅とし、上下では上顎洞粘膜側から口腔粘膜側にかけて観察を行った。

6. 統計学的処理

2 群間の比較には Student の t 検定、複数の群間の比較には Tukey の方法、いずれも $p < 0.05$ において検定を行った。なお本研究は、日本歯科大学倫理審査委員会の承認 (NDU-T2015-20) を得て、献体の扱いは献体法と死体解剖保存法に遵守して行った。

結果

1. 骨構造の分析

上顎洞粘膜側皮質骨は有歯顎と遊離端欠損、有歯顎と無歯顎、中間歯欠損と遊離端欠損、中間歯欠損と無歯顎、口腔粘膜側皮質骨は有歯顎と中間歯欠損、有歯顎と遊離端欠損、有歯顎と無歯顎、中間歯欠損と無歯顎、遊離端欠損と無歯顎で有意差が認められた（図 6）。性差では、有歯顎の口腔粘膜側皮質骨で有意差が認められた（図 7）。

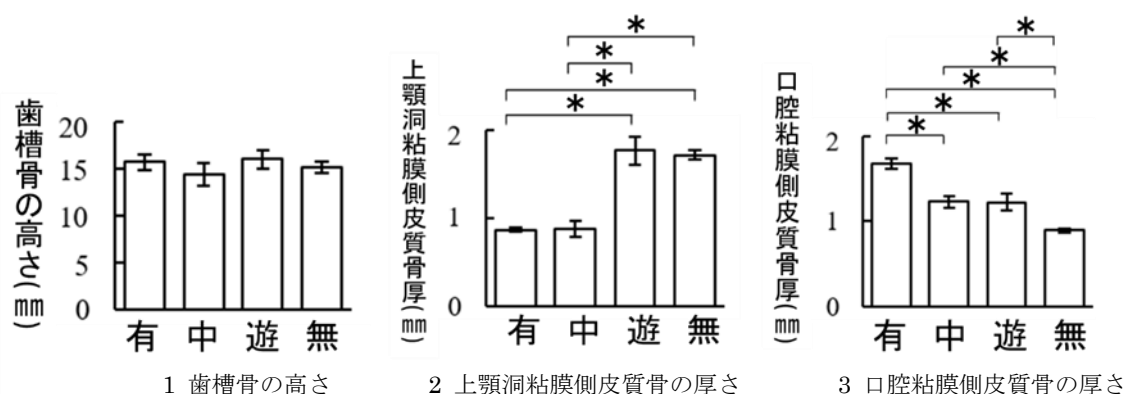


図 6 骨構造の計測（全体）

有：有歯顎、中：中間歯欠損、遊：遊離端欠損、無：無歯顎、*： $p < 0.05$

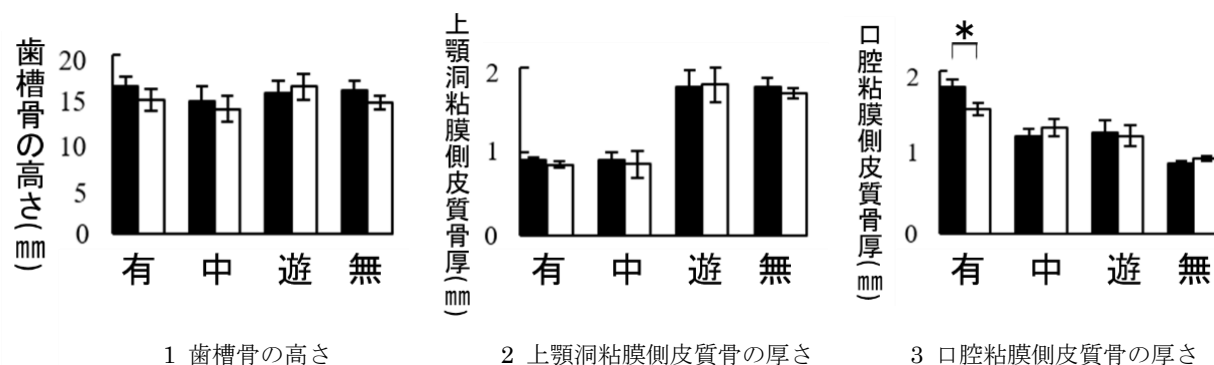


図 7 骨構造の計測（性別）

■：男性、□：女性、有：有歯顎、中：中間歯欠損、遊：遊離端欠損、無：無歯顎、*： $p < 0.05$

2. 骨梁構造の分析

S1 は有歯顎と中間歯欠損、S3 は遊離端欠損と無歯顎で高い比率となった（図 8）。

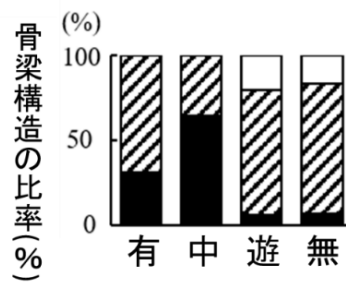


図8 骨梁構造の評価 (全体)

■ : S1、▨ : S2、□ : S3、有 : 有歯顎、中 : 中間歯欠損、遊 : 遊離端欠損、無 : 無歯顎

3. 骨密度の分析

骨密度の分析では、有歯顎と中間歯欠損、有歯顎と遊離端欠損、有歯顎と無歯顎、中間歯欠損と遊離端欠損、中間歯欠損と無歯顎で有意差が認められた。性差は、有歯顎と中間歯欠損で男性が女性よりも有意に高かった (図9)。

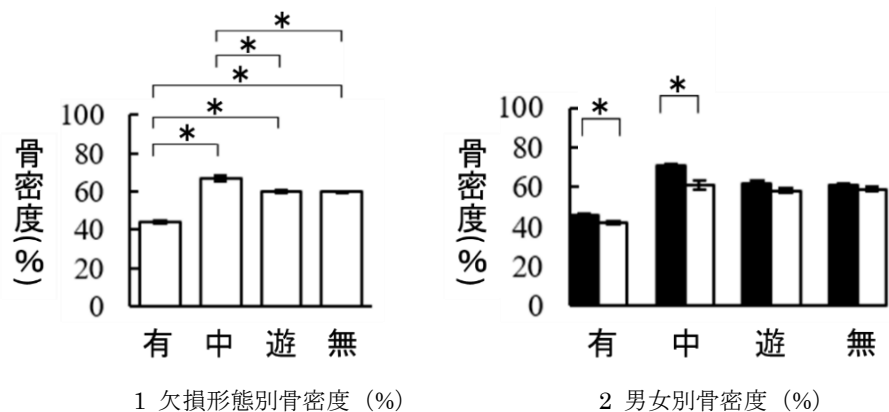


図9 骨密度の評価 (全体・性別)

■ : 男性、□ : 女性、有 : 有歯顎、中 : 中間歯欠損、遊 : 遊離端欠損、無 : 無歯顎、* : $p < 0.05$

4. 組織学的所見

HE 染色では、上顎洞粘膜側の有歯顎と中間歯欠損は薄い皮質骨、遊離端欠損と無歯顎は厚い皮質骨、海綿骨は有歯顎と中間歯欠損は厚くコンパクトな骨梁に小さい骨小窩や骨髓腔、遊離端欠損と無歯顎は薄く伸びた骨梁に大きい骨髓腔、口腔粘膜側の有歯顎と中間歯欠損は厚い皮質骨、遊離端欠損と無歯顎は薄い皮質骨が認められた (図10、11)。

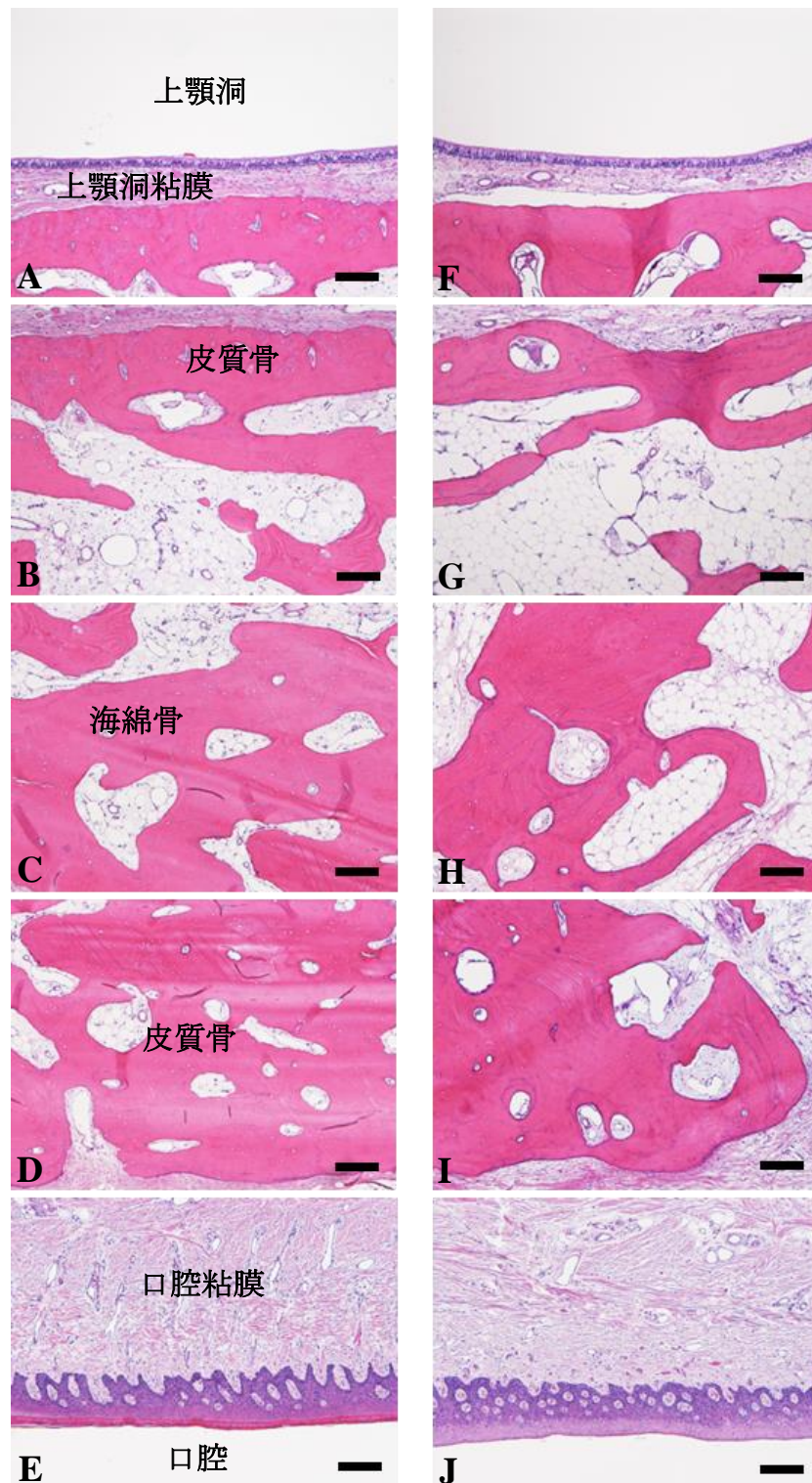


図 10 HE 染色所見 (有歯顎・中間歯欠損)

A～E：有歯顎、F～J：中間歯欠損、A・F：上顎洞粘膜側、B・G：上顎洞粘膜側皮質骨、
C・H：海綿骨、D・I：口腔粘膜側皮質骨、E・J：口腔粘膜側、バー＝200 μ m

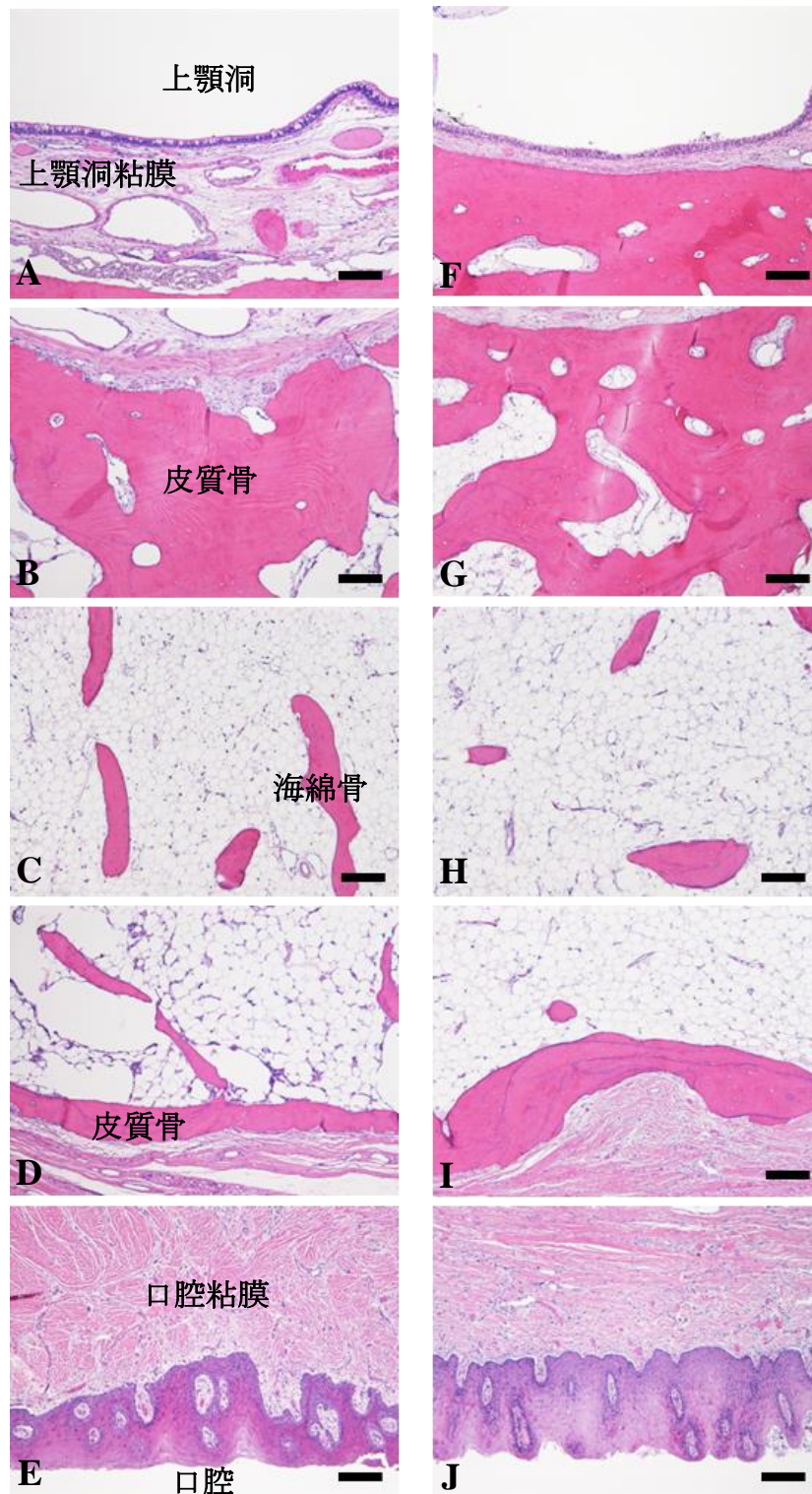


図 11 HE 染色所見（遊離端欠損・無歯顎）

A～E：遊離端欠損、F～J：無歯顎、A・F：上顎洞粘膜側、B・G：上顎洞粘膜側皮質骨、
C・H：海綿骨、D・I：口腔粘膜側皮質骨、E・J：口腔粘膜側、バー＝200 μm

CD31 免疫染色による特徴は、上顎洞粘膜側の有歯顎と中間歯欠損では小さな丸い血管が散在性に、遊離端欠損は大小多くの血管が、無歯顎は少量の小さい丸い血管、海綿骨部分は有歯顎、中間歯欠損、遊離端欠損、無歯顎共に様々な形の血管、口腔粘膜側の有歯顎と中間歯欠損は様々な形の多くの血管が、遊離端欠損と無歯顎では少量の小さく丸い血管が走行して骨組織の中に認められた。また中間歯欠損、遊離端欠損、無歯顎では、有歯顎に比較して脂肪細胞が多くみられ、とくに無歯顎で多く認められた（図 12、13）。

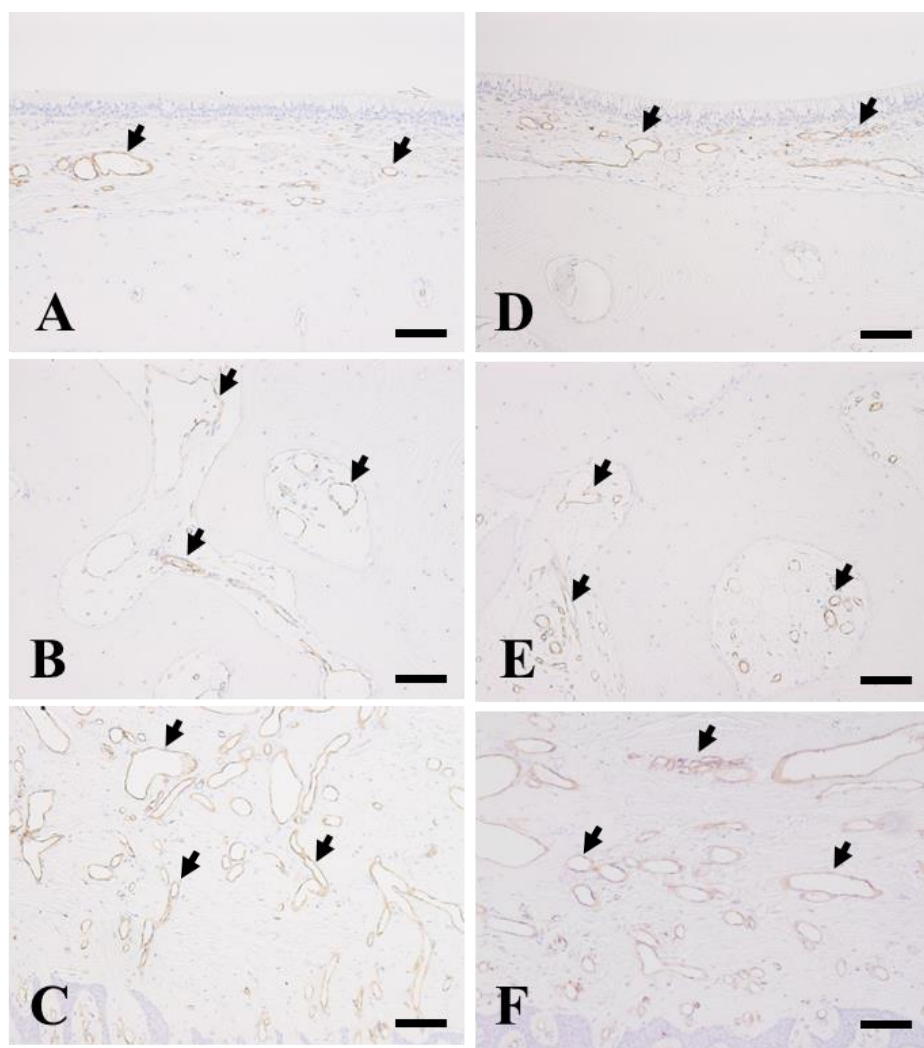


図 12 CD31 免疫染色所見（有歯顎・中間歯欠損）

A、D：CD31 陽性の小（直径 $50\mu\text{m}$ 以下）～中（およそ直径 $100\mu\text{m}$ ）の血管が上顎洞粘膜付近に散在的に観察される（矢印）、B・E：小～大（直径 $300\mu\text{m}$ 以上）の CD31 陽性の血管が海綿骨部分に観察される（矢印）、C・F：小～大の多くの CD31 陽性の血管が口腔粘膜付近に観察される（矢印）、A～C：有歯顎、D～F：中間歯欠損、A・D：上顎洞粘膜側、B・E：海綿骨、C・F：口腔粘膜側、バー＝ $100\mu\text{m}$

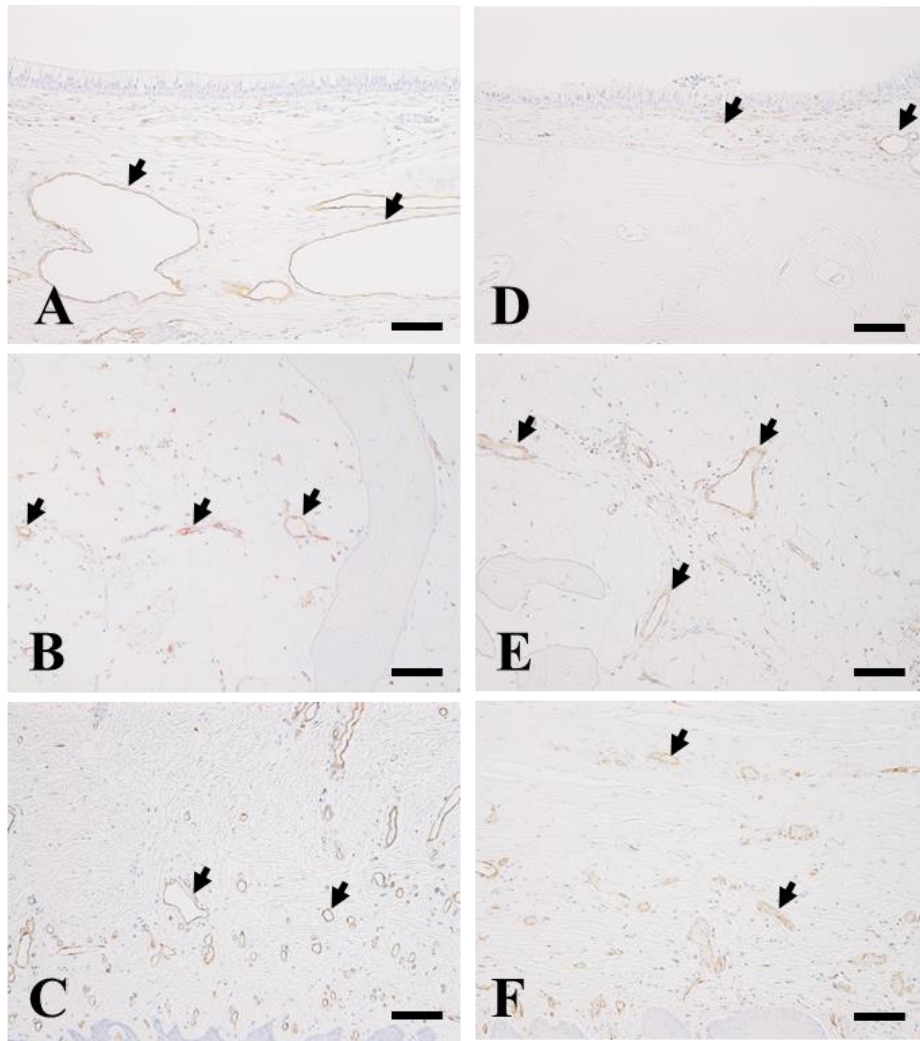


図 13 CD31 免疫染色所見（遊離端欠損・無歯顎）

A：上顎洞粘膜下に広がった大きな CD31 陽性血管が観察される（矢印）、D：上顎洞粘膜下に CD31 陽性の小さい血管が観察される（矢印）、B・C・E・F：海綿骨内および口腔粘膜付近に小さいあるいは中等度の血管が散在性に観察される（矢印）、A～C：遊離端欠損、D～F：無歯顎、A・D：上顎洞粘膜側、B・E：海綿骨、C・F：口腔粘膜側、バー＝100μm

考 察

NIH Consensus Development Panel (2001)²⁸⁾によると、“骨強度”の指標は骨構造などを含む骨質と骨密度で定義されている。骨強度の診断において、エックス線写真を使った分析は有効な方法の一つである²⁹⁾。上顎骨は中顔面を構成し、歯が喪失すると前頭骨、頬骨、口蓋骨が縫合部で癒合し、緻密骨が薄いことから形態的变化を受けやすく、また骨の中でも

複雑で特異的な三角錐に似た形で、その中心となっている頬骨下稜部付近には咀嚼筋も付着しているため³⁰⁾、外傷や咬合力によってその中心部には大きな力がかかると考えられる。さらに頬骨下の上顎骨に位置する第一大臼歯には歯の中でもとくにメカニカルストレスがかかり、その歯が失われると上顎骨のバランスを維持するためにその周囲の支持骨が重要な役割を担っている。そこで今回は、上顎第一大臼歯を中心に歯の欠損状態によって有歯顎と基準とし、中間歯欠損、遊離端欠損、無歯顎の4タイプに分けて骨の変化について放射線・組織学的に観察した。

皮質骨は、有歯顎と比較し上顎洞粘膜側皮質骨は遊離端欠損、無歯顎で厚く、口腔粘膜側皮質骨では中間歯欠損、遊離端欠損、無歯顎で薄かった。遊離端欠損、無歯顎では、上顎洞粘膜側皮質骨が厚くなっており、歯の喪失により上顎骨と縫合している周囲骨に依存し、頭蓋骨全体に分散して支えられているためであると考えられた。この結果は歯が多く喪失していることで、周囲骨へのストレスが強くなっていることを示していると考えられた。一方で、口腔粘膜側皮質骨の厚さの減少は、歯の喪失のための骨吸収によるものと考えられた。

海綿骨は、有歯顎の骨構造は、骨梁が太く、厚い層板状で網目構造を呈しており、力学的な強度を高めていると考えられた。これは垂直的な咬合力、ねじれや側方運動、筋肉などによる引っ張りなどに対応していると考えられる。有歯顎は歯に力が伝わることで、歯槽骨への力の負担が最も大きいと考えられ、歯槽骨の骨梁構造の発達が著しいと考えられた。中間歯欠損の骨構造は有歯顎と比較して、薄い層板状ではあったが、上下、左右共に骨梁構造は残存していた。中間歯欠損は前後に歯が存在するために、他の欠損形態と比較して顎骨の変化が少ないと考えられる。すなわち中間歯欠損は他の欠損形態と比較して、骨は垂直的および水平的な力のどちらにも対応できると考えられた。過去の報告^{17, 21, 31)}においても、歯科治療とくにインプラント治療において、両隣在歯に支えられた中間歯欠損部の骨は、上部構造が装着された後も骨吸収が少なく有利な状態であることが放射線学的、また組織学的に裏付けていると考えられた。

一方、遊離端欠損の骨構造は、咬合平面に垂直の縦長で細い骨梁構造が確認され、有歯顎の骨梁構造とは異なっていた。遊離端欠損の場合、とくに歯列の遠心において垂直方向の力が大きくかかると考えられるため、負荷の加わりにくい水平方向の骨梁構造が喪失し

でも、垂直方向の骨梁構造は残存していたと考えられた。すなわち、遊離端欠損は垂直的な力には強いが、水平的な力には弱いと考えられた。無歯顎の骨構造は、遊離端欠損同様に有歯顎の骨梁構造とは異なり、細かい砂状の骨構造が大半を占めていた。多数歯を喪失することによって、周囲骨に与える影響は他の欠損形態と比較して最も大きいと考えられ、骨梁構造の全体の改造が行われると考えられた。無歯顎における骨構造は全体的に細く小さくまばらであり、他の欠損形態と比較しても、垂直的な力、水平的なストレスに影響を受けやすい状態であると考えられた。

骨密度の観察手法について、CBCT はヘリカル CT と比較して患者への放射線被爆が少なく、骨梁構造の診断において優れている²⁹⁾。今回の観察においては、CBCT の骨密度の再現性を補正するための指標⁹⁾を用いて骨密度の評価を試みた。Lekholm ら²⁷⁾は骨密度の診断方法として下顎骨前歯部の側方頭部エックス線写真からその骨の密度と骨梁構造を類推して放射線学的に4つに分類して評価を行っている。しかし臨床においては、Lekholm & Zarb 分類に従って側方頭部エックス線写真から放射線学的に皮質骨、海綿骨の状態を推測することは極めて難しい。そこで骨強度の診断においてはさらなる改良が必要であると考え、本研究では Lekholm & Zarb 分類に加え、CBCT による評価法を加えた。歯の欠損形態による骨密度の影響は、有歯顎と比較して中間歯欠損、遊離端欠損、無歯顎では有意に高かった。今回指標とした骨密度の判定基準は、インプラント治療の術前診断における骨性状の指標としすでに報告されている⁹⁾。しかし、CBCT による評価法では、放射線学的には中間歯欠損、遊離端欠損、無歯顎は有歯顎よりも高い骨密度が推測されたが、組織学的観察では無歯顎において骨組織の残存が少なく、放射線学的に骨密度や骨の性状を予測することは難しいと考えられた。骨密度のみで骨強度を判断することが難しいことは多くの報告^{6, 10, 32)}でなされていて、骨梁構造も併せて観察し的確な骨強度の診断をすることが重要であることが確認された。

一般的に骨のリモデリングは、周囲の力学的因子に大きく影響を受けることが知られている。骨に与えられたメカニカルストレスに対応して骨の吸収と添加が繰り返され、骨内ではその外力に抵抗しうる構造を備える Wolff の法則³³⁾に則ってターンオーバーがおこなわれている。また Frost らの提唱したメカノスタット (mechanostat) 理論³⁴⁾では、ひずみを感じるセンサーが骨に存在し、さまざまな刺激が骨芽細胞の分化および活性化を促す

と報告されている。歯の欠損形態の違いにおいても、骨のリモデリングの状態が異なる可能性があるが、経時的な骨のリモデリングについては献体による評価は難しい。そこで今回は、血管の形成と骨の形成には関係があると報告³⁵⁾されていることから、歯の喪失後の顎骨の血管の状態は骨のリモデリングの結果を示すものであると考え、歯の欠損形態別に血管の観察を行った。また脂肪細胞は造血を抑制すると報告³⁶⁾されている。そこで本研究では、歯の欠損が骨のリモデリングや性状に与える影響について、血管と脂肪細胞を中心に観察することを目的に、放射線学的な検討と対比して組織学的に検討をおこなった。

上顎軟組織における血管分布は、上顎洞粘膜付近の結合組織において有歯顎と比較して遊離端欠損では広がった大きな血管が散在して認められた。この結果は上顎洞周囲における粘膜の代謝活性が盛んで、歯の欠損に伴う補綴物や咬合ストレスによる骨の吸収と共に周囲骨が変化していることが想定された。海綿骨における脂肪細胞は、組織学的には有歯顎では多くは認められず骨内に血管が散在していたのに対し、無歯顎の上顎骨では多く観察された。有歯顎から歯を喪失した後の経過の中で、骨のリモデリングが生じ、骨髄組織から脂肪細胞に置き換わって脂肪変性が生じた結果であると考えられた。

以上の結果より、上顎大臼歯部における歯の欠損形態別に血管や脂肪細胞の分布を観察することにより、骨のリモデリングを推測することは極めて有用であると考えられた。

まとめ

献体 91 体 171 側の上顎大臼歯部を有歯顎、中間歯欠損、遊離端欠損、無歯顎の 4 タイプに分類し、歯科用コーンビーム CT (CBCT) を用いて放射線学的および組織学的に顎骨構造の評価を行い、以下の結果が得られた。

- 1) 上顎洞粘膜側の皮質骨は、有歯顎と比較して遊離端欠損、無歯顎で有意に厚かった。
- 2) 口腔粘膜側の皮質骨は、有歯顎と比較して中間歯欠損、遊離端欠損、無歯顎で有意に薄かった。
- 3) 骨梁構造はタイプによる差はなかったが、とくに中間歯欠損では有歯顎に類似した構造が認められた。
- 4) CBCT 画像による解析では、有歯顎と比較して、中間歯欠損、遊離端欠損および

無菌顎では、有意に骨密度が高い傾向が認められた。

- 5) CD31 免疫染色所見では、遊離端欠損の上顎洞粘膜側および有菌顎の口腔粘膜側の粘膜固有層において、CD31 陽性の血管が多数観察された。
- 6) 脂肪細胞はとくに無菌顎で多く認められた。
- 7) 中間歯欠損は遊離端欠損や無菌顎よりも骨構造が密であり、遊離端欠損や無菌顎では骨構造が疎である傾向が認められた。

本研究において利益相反はない。

参考文献

- 1) Schropp L, Wenzel A, Kostopoulos L, Karring T (2003) Bone healing and soft tissue contour changes following single-tooth extraction: a clinical and radiographic 12-month prospective study. *Int J Periodontics Restorative Dent* 23: 313-323
- 2) Cardaropoli G, Araujo M, Lindhe J (2003) Dynamics of bone tissue formation in tooth extraction sites. An experimental study in dogs. *J Clin Periodontol* 30: 809-818
- 3) Araujo MG, Lindhe J (2005) Dimensional ridge alterations following tooth extraction. An experimental study in the dog. *J Clin Periodontol* 32: 212-218
- 4) Covani U, Ricci M, Bozzolo G, Mangano F, Zini A, Barone A (2011) Analysis of the pattern of the alveolar ridge remodelling following single tooth extraction. *Clin Oral Implants Res* 22: 820-825
- 5) Croucher PI, Garrahan NJ, Compston JE (1996) Assessment of cancellous bone structure: comparison of strut analysis, trabecular bone pattern factor, and marrow space star volume. *J Bone Miner Res* 11: 955-961
- 6) Muller R, van Campenhout H, van Damme B, van Der Perre G, Dequeker J, Hildebrand T, Rueggsegger P (1998) Morphometric analysis of human bone biopsies: a quantitative structural comparison of histological sections and micro-computed tomography. *Bone* 23: 59-66
- 7) Cortet B, Chappard D, Boutry N, Dubois P, Cotten A, Marchandise X (2004) Relationship between computed tomographic image analysis and histomorphometry for microarchitectural characterization of human calcaneus. *Calcif Tissue Int* 75: 23-31

- 8) Chappard D, Retailleau-Gaborit N, Legrand E, Basle MF, Audran M (2005) Comparison insight bone measurements by histomorphometry and microCT. *J Bone Miner Res* 20: 1177-1184
- 9) Naitoh M, Hirukawa A, Katsumata A, Aiji E (2010) Prospective study to estimate mandibular cancellous bone density using large-volume cone-beam computed tomography. *Clin Oral Implants Res* 21: 1309-1313
- 10) de Oliveira RC, Leles CR, Lindh C, Ribeiro-Rotta RF (2012) Bone tissue microarchitectural characteristics at dental implant sites. Part 1: identification of clinical-related parameters. *Clin Oral Implants Res* 23: 981-986
- 11) Blok Y, Gravesteyn FA, van Ruijven LJ, Koolstra JH (2013) Micro-architecture and mineralization of the human alveolar bone obtained with micro CT. *Arch Oral Biol* 58: 621-627
- 12) Gonzalez-Garcia R, Monje F (2013) Is micro-computed tomography reliable to determine the microstructure of the maxillary alveolar bone? *Clin Oral Implants Res* 24: 730-737
- 13) Ibrahim N, Parsa A, Hassan B, van der Stelt P, Aartman IH, Wismeijer D (2014) Accuracy of trabecular bone microstructural measurement at planned dental implant sites using cone-beam CT datasets. *Clin Oral Implants Res* 25: 941-945
- 14) Dias DR, Leles CR, Batista AC, Lindh C, Ribeiro-Rotta RF (2015) Agreement between Histomorphometry and Microcomputed Tomography to Assess Bone Microarchitecture of Dental Implant Sites. *Clin Implant Dent Relat Res* 17: 732-741
- 15) Parsa A, Ibrahim N, Hassan B, van Der Stelt P, Wismeijer D (2015) Bone quality evaluation at dental implant site using multislice CT, micro-CT, and cone beam CT. *Clin Oral Implants Res* 26: e1-7
- 16) Monje A, Gonzalez-Garcia R, Monje F, Chan HL, Galindo-Moreno P, Suarez F, Wang HL (2015) Microarchitectural pattern of pristine maxillary bone. *Int J Oral Maxillofac Implants* 30: 125-132
- 17) Pramstraller M, Farina R, Franceschetti G, Pramstraller C, Trombelli L (2011) Ridge dimensions of the edentulous posterior maxilla: a retrospective analysis of a cohort of 127 patients using computerized tomography data. *Clin Oral Implants Res* 22: 54-61

- 18) Farina R, Pramstraller M, Franceschetti G, Pramstraller C, Trombelli L (2011) Alveolar ridge dimensions in maxillary posterior sextants: a retrospective comparative study of dentate and edentulous sites using computerized tomography data. *Clin Oral Implants Res* 22: 1138-1144
- 19) Kopecka D, Simunek A, Brazda T, Rota M, Slezak R, Capek L (2012) Relationship between subsinus bone height and bone volume requirements for dental implants: a human radiographic study. *Int J Oral Maxillofac Implants* 27: 48-54
- 20) Monje A, Monje F, Gonzalez-Garcia R, Galindo-Moreno P, Rodriguez-Salvanes F, Wang HL (2014) Comparison between microcomputed tomography and cone-beam computed tomography radiologic bone to assess atrophic posterior maxilla density and microarchitecture. *Clin Oral Implants Res* 25: 723-728
- 21) Sharan A, Madjar D (2008) Maxillary sinus pneumatization following extractions: a radiographic study. *Int J Oral Maxillofac Implants* 23: 48-56
- 22) Bertl K, Heimel P, Rokl-Riegler M, Hirtler L, Ulm C, Zechner W (2015) MicroCT-based evaluation of the trabecular bone quality of different implant anchorage sites for masticatory rehabilitation of the maxilla. *J Craniomaxillofac Surg* 43: 961-968
- 23) Razavi R, Zena RB, Khan Z, Gould AR (1995) Anatomic site evaluation of edentulous maxillae for dental implant placement. *J Prosthodont* 4: 90-94
- 24) Trisi P, Rao W (1999) Bone classification: clinical-histomorphometric comparison. *Clin Oral Implants Res* 10: 1-7
- 25) Ulm C, Kneissel M, Schedle A et al (1999) Characteristic features of trabecular bone in edentulous maxillae. *Clin Oral Implants Res* 10: 459-467
- 26) Misch CE (2015) Dental Implant Prosthetics, second edition. In: Misch CE Bone Density. Elsevier Health Sciences, St. Louis, Missouri: pp 237-252
- 27) Lekholm U, Zarb GA (1985) Patient selection and preparation. In: Branemark PI, Zarb GA, Albrektsson T (eds) Tissue integrated prostheses: osseointegration in clinical dentistry. Quintessence, Chicago, pp 199–209
- 28) NIH Consensus Development Panel (2001) Osteoporosis prevention, diagnosis, and therapy. *Jama* 285: 785-795

- 29) White SC, Pharoah MJ (2014) Oral Radiology: Principles and Interpretation, seventh edition. In: White SC Cone-Beam Computed Tomography. Elsevier Health Sciences, St. Louis, Missouri: pp 185-213
- 30) Berkovitz BKB, Holland GR, Moxham BJ (2009) Oral anatomy, histology and embryology. In Regional topography of the mouth and related areas, 4th Edition. Mosby/Elsevier, New York, pp 66-69
- 31) Pabst AM, Walter C, Ehbauer S, Zwiener I, Ziebart T, Al-Nawas B, Klein MO (2015) Analysis of implant-failure predictors in the posterior maxilla: a retrospective study of 1395 implants. J Craniomaxillofac Surg 43: 414-420
- 32) Wirth AJ, Goldhahn J, Flaig C, Arbenz P, Muller R, van Lenthe GH (2011) Implant stability is affected by local bone microstructural quality. Bone 49: 473-478
- 33) Wolff J (1986) The law of Bone Remodeling. Springer, Germany
- 34) Frost HM (1987) Bone "mass" and the "mechanostat": a proposal. Anat Rec 219: 1-9
- 35) Kusumbe AP, Ramasamy SK, Adams RH (2014) Coupling of angiogenesis and osteogenesis by a specific vessel subtype in bone. Nature. 507:323-328
- 36) Naveiras O, Nardi V, Wenzel PL, Hauschka PV, Fahey F, Daley GQ (2009) Bone-marrow adipocytes as negative regulators of the haematopoietic microenvironment. Nature 460: 259-263

Histological and radiographic study of human edentulous and dentulous maxilla

Yukino Kamigaki, Iwao Sato, Takashi Yosue

Short running title: Morphology of human maxilla

Abstract

Data on the bone trabecular structure and density of the edentulous regions of the first upper molars are important for designing successful dental treatments, especially dental implants. However, no detailed defined morphometric properties on the human maxilla are available at the immunohistochemical and radiographic levels. Cone-beam computed tomography analysis and immunohistochemical observation were applied to the maxillary first molar region of 91 cadavers (46 males and 45 females). The edentulous maxilla can be classified into the following three forms: fully edentulous (FE), partially edentulous (PE), and immediately edentulous (IE). Compared with the first molar dentulous (FMD) specimens, significant differences in cortical bone height and bone density exist among IE, PE, and FE in maxilla ($p < 0.001$). According to histochemical observations, the positive CD31 reaction clearly described a large vessel of the PE maxilla and small vessels of FMD and IE in maxillary sinus connective tissue. These structural issues were clearly related to tooth extraction. These morphological and radiographic data describing the edentulous region of the maxillary first molar might be useful for improving dental treatments.

Keywords: human alveolar bone, bone structure, bone density, CBCT, CD31

Introduction

Tooth extraction causes changes in the bone matrix of the maxilla. In general, the height of the buccal wall tends to decrease and the bundle bone disappears leading to a reduced height and width of the residual ridge (Schropp et al. 2003; Cardaropoli et al. 2003; Araújo and Lindhe 2005; Covani et al. 2010). Moreover, internal structures, such as the trabecular bone of the maxilla, are strongly affected by tooth extraction. Intrabone evaluation of the quality and the quantity of bone is among the factors affecting the success of dental treatments, especially dental implants. Computed tomography (CT) provides a useful quantification of bone density if expressed in Hounsfield units according to calibrated gray-level scale methods. Cone-

beam computed tomography (CBCT) also has advantages in terms of cost, time, image resolution, and radiation information. CBCT provides useful information regarding bone density characteristics in the form of three-dimensional gray-scale images (Parsa et al. 2012). Lekholm and Zarb (Lekholm and Zarb 1985) indicated four types of bone quality in anterior regions of the jaw: homogenous cortical bone (Type 1); a thick layer of cortical bone surrounding a central part of dense trabecular bone (Type 2); a thin layer of cortical bone surrounding dense trabecular bone of favorable strength (Type 3); and a thin layer of cortical bone surrounding low-density trabecular bone (Type 4). However, it is difficult to adapt the Lekholm and Zarb classification to the complex maxillary bone structure, which can be thin around the maxillary sinus.

A morphometric analysis includes various measurements, such as bone volumetric fraction, bone mineral density of the cortical bone and trabecular bone, trabecular thickness, trabecular spaces, trabecular number, and trabecular structure (Croucher et al. 1996; Muller et al. 1998; Cortet et al. 2004; Chappard et al. 2005; Naitoh et al. 2010; de Oliveira et al. 2012; Blok et al. 2013; Dias et al. 2015; Gonzalez-Garcia and Monje 2013; Ibrahim et al. 2014; Parsa et al. 2015; Monje et al. 2015). In the maxilla, investigators have reported on bone height and bone width (Pramstraller et al. 2011; Farina et al. 2011; Kopecka et al. 2012; Monje et al. 2014). The characteristic features of bone morphology and histochemical structures differ in the edentulous human maxilla (Razavi et al. 1995; Trisi and Rao 1999; Ulm et al. 1999). Bone biological evaluation (immunohistochemistry and mRNA levels) differs between Types 1 and 2, according to the Lekholm and Zarb classification, in human mandibular alveolar bone. Moreover, bone healing with synostosis is a complex process involving an inflammatory response, angiogenesis, and osteogenesis (Davies 2003; Donos et al. 2011). These specific biological properties of the maxillary bone may cause difficulty in evaluating bone for dental implant treatments.

After tooth extraction occurs in the maxillary first molar region, the structural pattern can be classified into four forms (Kennedy's Classification): dentulous (FMD), fully edentulous (FE), partially edentulous (PE) and immediately edentulous (IE) (Kennedy 1928). The PE has an apparent higher inadaptability than that of the IE at the maxillary alveolar crest height in dental treatments, despite there being no histological and morphological data for PE and IE using CT (Pramstraller et al. 2011; Sharan and Madjar 2008). Moreover, previous reports indicated the difference in bone quality and quantity between the anterior and posterior regions of the maxilla using micro-CT only (Monje et al. 2015; Bertl et al. 2015; Blok et al. 2013).

Intrabone quality and quantity have not been evaluated in these edentulous forms. The intrabone characteristics of various forms may affect the planning of dental implant treatments.

The maxillary first molar region is an important site of occlusion, which is maintained by implant placement (Goto et al. 2012). Moreover, because the bone trabecular structure and density affect bone volume, dental implant treatments have a major impact on prognosis clinical treatment (Martinez et al. 2001; Marquezan et al. 2012). For stabilization of the implant body after implantation, the relationship between osseointegration and vascularization is known to be important (Civelek et al. 1995; Davies 2003). Vascularization is also important for dental implantation (Scardina et al. 2011). Vascularization is a marker for osseointegration in dental implants. However, previous reports provided no information regarding the localization of blood vessels and bone quality levels. Therefore, upon analyzing the vascularization, we attempted to identify blood vessels using the vascular endothelial cell marker, CD31 (Ilan and Madri 2003; Pusztaszeri et al. 2006) to distinguish between fat cells and blood vessels in the bone marrow.

We attempted to investigate the bone quality and quantity of these four forms in the maxillary first molar region. Moreover, we also defined the morphometric properties of these four forms of bone quality using immunohistochemistry and radiography to provide information regarding the location of blood vessels, connective tissues, and fatty trabecular bone. These results provided useful information about the maxillary structure and helped with the planning of dental treatments.

Materials and Methods

Specimen collection and grouping

A total of 171 specimens in 91 cadavers that were preserved in the Department of Anatomy of the Nippon Dental University were used in this study. Forty-six male cadavers (59-93 years old; mean $78.8 \pm \text{SD } 8.29$) yielded 85 specimens; 44 specimens were from the right side, and 41 were from the left side. Forty-five female cadavers (61-103 years old; mean $85.6 \pm \text{SD } 8.77$) yielded 86 specimens; 43 specimens were from the right side, and 43 were from the left side). The maxillary first molar region was investigated. Bone disease, especially osteoporosis (Barngkgei et al. 2014), and partially damaged or already dissected maxilla were excluded from our study. We assessed and classified the specimens based on the four forms of

Kennedy's Classification as follows: FMD, 17 males (8 right side, 9 left side) and 17 females (8 right side, 9 left side); IE, 11 males (5 right side, 6 left side) and 17 females (8 right side, 9 left side); PE, 26 males (14 right side, 12 left side) and 22 females (12 right side, 10 left side) and FE, 31 males (17 right side, 14 left side) and 41 females (20 right side, 21 left side) (Fig. 1). The specimens were selected according to the following inclusion criteria for alveolar bone (these criteria have resulted in long-term dental implant success): height, more than 5 mm; width, more than 6 mm; and mesiodistal, more than 7 mm (Misch 2015).

CBCT analysis

Images of the maxillary first molar region were obtained using CBCT (AZ 3000CT; Asahi Roentgen Industry, Kyoto, Japan). Cone beam scans were performed for the maxillary first molar region using a tube potential of 85 kV, a tube current of 4 mA, and cylindrical data of 79 mm ϕ \times 80 mm at high resolution (voxel size 0.155 \times 0.155 \times 0.155 mm). Three-dimensional image observation was performed using NEOPREMIUM software (Asahi Roentgen Industry, Kyoto, Japan). The images were observed to confirm the identity of the median sagittal plane and the palatal plane as a reference plane. Then, the frontal section was explored from the infrazygomatic crest for the IE, PE, and FE specimens; the FMD specimens were explored from the center of the first and second molars (Fig. 1).

Analysis of bone structure

Measurements were assessed using ImageJ 1.48 (U. S. National Institutes of Health). On cross-sectional images, the height (the maxillary first molar region from the bottom of the maxillary sinus to the oral mucosa at a right angle to the palatal plane) was measured. The thickness of the cortical bone on the maxillary sinus side and the thickness of the cortical bone on the oral mucosa side were measured (Fig. 2A).

We classified three types (S1-3) of bone structure in the first molar regions of the four forms of the maxilla (FMD, IE, PE and FE) as follows: Type S1, a thin layer of cortical bone surrounding dense trabecular bone of favorable strength (Lekholm and Zarb classification Type 3); Type S2, a thin layer of cortical bone surrounding low-density trabecular bone (Lekholm and Zarb classification Type 4); Type S3, very soft bone with few incompletely mineralized trabecular bones (IM) or large intertrabecular spaces (LIS) (no type in the Lekholm and Zarb classification) (Fig. 3). The image was scored from Type S1 to S3

based on the bone structure of the cancellous bone (Fig. 3).

Analysis of bone density

Bone density was measured using ImageJ 1.48. Measurements were made of the cancellous bone area (Fig. 2B-1). A reference bone block of 200 mg/cm³ of hydroxyapatite was simultaneously scanned when obtaining the CBCT images. Based on the reference bone block, all specimens were converted into binary images (Fig. 2B-2).

Immunohistochemical methods

After washing four forms of the maxillary first molar regions (each form n=4) with PBS for 30 min at room temperature, the specimens were decalcified with 10% EDTA-PBS for 21-36 days at 4°C. The specimens were then washed with PBS for 30 min. The specimens were fixed using 70% alcohol and then dehydrated using the normal method. That is, paraffin-embedded blocks and sections of human maxilla for use in the immunohistochemistry experiments were obtained; 16 samples (four samples each of FE, PE, IE and FMD; male mean age 80.4± SD 7.61 years old) were obtained from Genostaff Co., Ltd. (Tokyo, Japan) and decalcified. These samples were fixed with tissue fixative (Genostaff Co., Ltd. Tokyo, Japan), embedded in paraffin using Genostaff's proprietary procedures, and sectioned at 8 µm. The tissue sections were deparaffinized using xylene and rehydrated using a series of ethanol solutions in PBS. Endogenous peroxidase was blocked using 0.3% H₂O₂ in methanol for 15 min, followed by incubation with G-Block (Genostaff Co., Ltd. Tokyo, Japan) and an Avidin/Biotin Blocking Kit (Vector SP-2001, Vector Laboratory, CA, USA). The sections were incubated with 0.4 µg/ml of anti-CD31 antibody (1:500; Lab Vision Corp, CA, USA; catalogue number #RB-10333) at 4°C overnight. Rabbit immunoglobulin fraction (Dako X0936, Takasaki, Japan) was used as a negative control. After washing with TBS, biotin-conjugated goat anti-rabbit immunoglobulin (Dako, Takasaki, Japan) was added at 1:600 dilution, and the mixture was incubated for 30 min at room temperature, after which peroxidase-conjugated streptavidin (Nichirei, Tokyo, Japan) was added for 5 min. Peroxidase activity was visualized using diaminobenzidine. The sections were counterstained using Mayer's hematoxylin and eosin (Muto, Tokyo, Japan), dehydrated and then mounted using malinol. The stained sections were evaluated under a microscope (DM-2500; Leica Microsystems,

Germany).

Statistical analysis

The differences in bone structure and density among the forms were assessed using Student's test and two-way analysis of variance (ANOVA), followed by Tukey's post-hoc test. Differences were considered significant when $p < 0.05$. The results are reported as the means \pm SD.

Ethics

The study was approved by the Human Research Committee of Nippon Dental University (no. NDU-T2015-20). The human cadavers were obtained from a donor-based system using the guidelines included with the Law Concerning Body Donation for Medical and Dental Education (the Body Donation Law) and the Law Concerning Cadaver Dissection and Preservation (LCCDP).

Results

Analysis of bone structure

We examined the bone structure of the various forms according to Kennedy's classification, bone structure and height (the maxillary first molar region from the bottom of maxillary sinus to the oral mucosa, at a right angle to the palatal plane), the thickness of cortical bone from the maxillary sinus side (TMS), the thickness of cortical bone from the oral mucous side (TOM) and the percentage of the three bone types (S1, S2, and S3). Figure 4A and 4E show that bone height did not significantly differ among the four forms. The TMS of PE and FE was higher than that of FMD ($p < 0.001$), and a significant difference in thickness was observed between IE and PE or between IE and FE ($p < 0.001$); in contrast, no significant difference was found between FMD and IE or between PE and FE (Fig. 4B). The TMS values of PE and FE were high compared to those of FMD and IE (Fig. 4B). TOM also showed a significant difference in thickness between FMD and IE, between FMD and PE, between FMD and FE, between PE and FE ($p < 0.001$), and between IE and FE ($p < 0.01$); in contrast, no significant difference was found between IE and PE (Fig. 4C). The TOM of IE, PE, and FE were low compared to that of FMD (Fig. 4C). In Figure 4D, FMD and IE were scored as Type S1 at a higher rate than were PE and FE. In contrast, PE and FE were scored as Type S3 at

a higher rate. Height and TMS were not significantly different between males and females for all four forms (Fig. 4E, F). In contrast, thickness differed more significantly between males and females in FMD in comparison to the others ($p<0.05$) (Fig. 4G).

Moreover, no statistically significant difference was found between right and left bone structure and density in the examined samples.

Analysis of bone density

We examined bone density in the various forms according to Kennedy's classification. Bone density differed significantly between FMD and IE, between FMD and PE, between FMD and FE, between IE and PE, and between IE and FE ($p<0.001$); in contrast, bone density did not significantly differ between PE and FE (Fig. 5A). The bone density of FMD was significantly lower than that of the other forms ($p<0.001$) (Fig. 5A). The bone density of males was higher than that of females for FMD and IE ($p<0.01$) in comparison to the others (Fig. 5B).

Moreover, no statistically significant difference was found between right and left bone structure and density in the examined samples.

Histochemical observation

After hematoxylin and eosin staining, the structure of the trabecular bone indicated various features in the FMD, IE, PE and FE of the human maxilla (frontal section). At the maxillary sinus side, thin cortical bone was found in FMD and IE; in contrast, thick cortical bone was found in PE and FE. In cancellous bone, compacted trabecular bone with small bone lacunae and small amounts of bone marrow were found in FMD and IE; in contrast, thin, elongated trabecular bone with large amounts of bone marrow were found in PE and FE. In the bone marrow, few fatty-like cells were observed in FMD; however, in PE and FE, many fatty-like cells were observed in the bone marrow of the maxilla. In the bone marrow of the FMD, few adipose tissues were observed; in contrast, rich fatty-like cell layers were observed in the bone marrow of PE and FE. At the oral mucosa side, thick cortical bone was found in FMD and IE; in contrast, thin cortical bone was found in PE and FE (Figs. 6 and 7).

Anti-CD31-positive vessels; their structure and localization in the four forms

Various anti-CD31-positive vessels were found in the FMD, IE, PE and FE of the human maxilla. At the maxillary sinus side, several small ($> 50 \mu\text{m}\phi$) oval vessels ("several" indicates between 2-3 and 50 vessels per mm^3) were scattered in the thin connective tissue layer and the cortical bone of FMD and IE; in contrast, many small and large ($<300 \mu\text{m}\phi$) vessels ("many" indicates <50 per mm^3) were present in the PE, and a few small oval vessels ("few" indicates 2-3 per mm^3) were present in the FE. In the middle region of the maxilla, many elongated and small oval vessels were found in the cancellous bone of all examined specimens. Moreover, many elongated and small oval vessels were also found in the fatty layer of the cancellous bone in IE, PE and FE (but not in FMD). At the oral mucosa side, many elongated and oval vessels were found in the connective tissue layer and in the cortical bone of FMD and IE; in contrast, small oval vessels were found in PE and FE (Figs. 8-11).

Discussion

According to the National Institute of Health (NIH) Consensus Development Panel, an indicator of "bone strength" is defined in terms of bone density and quality (NIH Consensus Development Panel 2001). For dental treatment purposes, bone strength can be evaluated using non-invasive X-radiation, which provides images of the alveolar bone and its volume, density and quality through CT and CBCT (White 2014). The bone trabecular structure and density of the maxilla were maintained by prosthetic treatments in dental implants. In addition, specific sutured connections with the frontal bone, zygomatic bone, and palatine bone may lead to mechanical stress in the maxilla. Therefore, it is necessary to compare each defect form because the balance is disturbed by defective teeth located in the maxilla.

In general, the maxilla adopts the shape of a triangular pyramid; the maxilla is complex and specific compared with other skull bones in suture connections. The first molar region is located at the zygomatic alveolar line portion and is susceptible to mechanical stress at the time of load (FE, PE and IE). In our results, we found a significant difference between the edentulous and dentulous samples. Therefore, this may be an important region for mechanical stress in occlusions.

Cortical bone structure observed in the four forms

Cortical bone is structurally denser and stronger than cancellous bone, and the structural content is likely to change under the influence of mechanical stress to constitute a bony circumference. In FMD, the cortical bone at the oral mucosa side can form a thick and compact structure that can support the teeth. On the other hand, the FE and PE of the cortical bone at the maxillary sinus side become thicker to maintain the strength of the entire skull through forming connective tissue with the suture between the maxilla and the frontal bone, zygomatic bone and palatine bone. Moreover, the decrease in the thickness of the cortical bone at the oral mucosa side in FE and PE may be due to bone absorption, which was caused by tooth loss.

Cancellous bone structure observed in the four forms

Mechanical stress may affect cancellous bone more than cortical bone (Billezikian et al. 1996). Therefore, the structure of cancellous bone is believed to be greatly susceptible to the mechanical strength of the bone. In FMD, the thick trabecular bone cortex adopts the form of a thick, compacted, layered plate, with mechanical vertical occlusal forces, torsion, lateral movement, mechanical stress, and tensile strength due to the muscles, which likely cause each force. Mechanical stress due to occlusion was considered a force applied to the trabecular bone in the cancellous bone, where the bone structure is dispersed. The survival rate of dental implants in IE are higher than those in FE and PE (Pabst et al. 2015). Previous reports have shown that PE is less adaptable than IE, although no histological and morphological data have been obtained for PE and IE using CT (Pramstraller et al. 2011; Sharan and Madjar 2008). Compared with FE and PE, IE was found in this study to be more adaptable when dental implant treatments are performed; these findings were obtained not only radiologically using CBCT but also histochemically. Compared with FMD, the bone structure of IE was shown to have a slightly thin, layered plate structure, and compacted trabecular bone was found in the bone marrow. In PE, thin trabecular bone, which was found to have high bone density despite the contrary histologic findings, was mostly present; this probably occurred because the trabecular bone was differently structured from the FMD. Most of the thin structure of the trabecular bone was arranged at right angles to the palatine in the bone marrow. This specific bone marrow structure suggested that the upper direction of the force in the centrifugal dentition maintained pressure on the cancellous bone. These cancellous bone trabecular structures are considered to avoid stress from the occlusion load. If the lateral direction of the trabecular bone pressure is lost, then the vertical direction of force is maintained in

the trabecular bone structure until bone marrow is lost. In the FE and PE, primarily thin trabecular bones were observed histologically. These thin trabecular bones were different from the bone structure of the FMD and IE. Through the loss of teeth, the occlusal pressure becomes weaker than the pressure on the adjacent palatine bone and other bones. In particular, in the FE, very thin trabecular bone is clearly shown to be weakened in response to the longitudinal force of occlusion.

Bone density in the four forms

In our results obtained using the modified CBCT methods, bone density was significantly lower in the FMD than in the other forms. This result is consistent with previous reports (Muller 2003; Wirth et al. 2011; de Oliveira 2012). In our results, bone density and trabecular structure were by evaluating bone structure and strength. The standard bone density and this evaluation are indicators of bone that can be commonly used in implant treatments to repair tooth defects during dental treatment (Naitoh et al. 2010). Moreover, edentulous forms, such as the IE, PE and FE, were shown to have higher bone density than the FMD. In particular, FE trabecular bone was thin; evaluation of bone using this method as the only indicator of bone density is difficult because the trabecular structure of cancellous bone is small, and the trabecular bone is thin.

In our results, a gender difference was found regarding bone density and the bone structure of the FMD and IE. This difference may relate to different mastication forces used by males and females in the human maxilla, although no difference was found histochemically. Further study of these gender differences is warranted.

Blood vessels in the four forms

Blood vessel morphology may affect the different forms of bone quality during remodeling. Marrow fat cells act as spacers between hematopoietic cells and bone tissue and function in lipid metabolism and energy storage. It has been suggested that bone marrow fat cells suppress the hematopoietic function to support hematopoiesis and bone metabolism (Lee and Karsenty 2008; Naveiras et al. 2009; Lecka-Czernik 2012; Krings et al. 2012). In our results, more large blood vessels were observed in the maxillary sinus mucosa around the connective tissues of the PE compared with those of the FMD and IE. The blood vessels were

subjected to anti-CD31 immunohistochemical staining, which helped to distinguish between marrow adipose tissue and blood vessels. Fat is important for bone quality, as shown in previous reports (Beresford et al.1992; Wang et al. 2016). In our results, FMD and IE appeared higher in quality compared to PE and FE. This might contribute to the adaptability of the IE forms in dental implants compared to PE and FE.

Conclusion

We analyzed the bone structure and density of the cortical and cancellous bone between the dentulous and edentulous first molar regions of the maxilla. The analysis was also performed for four forms of bone trabecular structure and density; FMD, IE, PE and FE. A specific and significant difference was found between the FMD forms and the edentulous groups in terms of bone trabecular structure and density. Moreover, vascularization in the connective tissue layer beneath the maxillary sinus mucosa and adipose tissue are important marker for the bone of the maxilla. This evaluation of bone structure and density may contribute to the knowledge base for dental implant treatments.

Acknowledgment: The authors declare their great appreciation for the staff of the Department of Anatomy of Nippon Dental University.

Our research was supported by Research Promotion Grants from Nippon Dental University (NDU GRANTS T-15001).

Conflict of Interest: None.

References

- Arau 'jo MG, Lindhe J (2005) Dimensional ridge alterations following tooth extraction. An experimental study in the dog. J Clin Periodontol 32: 212-218
- Barnkgel I, AL Haffar I, Khattab R (2014) Osteoporosis prediction from the mandible using cone-beam computed tomography. Imaging Sci Dent 44: 263-271

- Beresford JN, Bennett JH, Devlin C, Leboy PS, Owen ME (1992) Evidence for an inverse relationship between the differentiation of adipocytic and osteogenic cells in rat marrow stromal cell cultures. *J Cell Sci* 102 (Pt 2): 341-351
- Bertl K, Heimel P, Rokl-Riegler M, Hirtler L, Ulm C, Zechner W (2015) MicroCT-based evaluation of the trabecular bone quality of different implant anchorage sites for masticatory rehabilitation of the maxilla. *J Craniomaxillofac Surg* 43: 961-968
- Billezikian JP, Raisz LG, Rodan GA (1996) Principles of bone biology. Academic Press, San Diego, California, USA, pp 1135-1146: 1343-1354
- Blok Y, Gravesteijn FA, van Ruijven LJ, Koolstra JH (2013) Micro-architecture and mineralization of the human alveolar bone obtained with micro CT. *Arch Oral Biol* 58: 621-627
- Cardaropoli G, Araujo M, Lindhe J (2003) Dynamics of bone tissue formation in tooth extraction sites. An experimental study in dogs. *J Clin Periodontol* 30: 809-818
- Chappard D, Retaillieu-Gaborit N, Legrand E, Basle MF, Audran M (2005) Comparison insight bone measurements by histomorphometry and microCT. *J Bone Miner Res* 20: 1177-1184
- Civelek AC, Pacheco EM, Natarajan TK, Wagner HN, JR., Iliff NT (1995) Quantitative measurement of vascularization and vascular in growth rate of coralline hydroxyapatite ocular implant by Tc-99m MDP bone imaging. *Clin Nucl Med* 20: 779-787
- Cortet B, Chappard D, Boutry N, Dubois P, Cotten A, Marchandise X (2004) Relationship between computed tomographic image analysis and histomorphometry for microarchitectural characterization of human calcaneus. *Calcif Tissue Int* 75: 23-31
- Covani U, Ricci M, Bozzolo G, Mangano F, Zini A, Barone A (2011) Analysis of the pattern of the alveolar ridge remodelling following single tooth extraction. *Clin Oral Implants Res* 22: 820-825
- Croucher PI, Garrahan NJ, Compston JE (1996) Assessment of cancellous bone structure: comparison of strut analysis, trabecular bone pattern factor, and marrow space star volume. *J Bone Miner Res* 11: 955-961
- Davies JE (2003) Understanding peri-implant endosseous healing. *J Dent Educ* 67: 932-949

- de Oliveira RC, Leles CR, Lindh C, Ribeiro-Rotta RF (2012) Bone tissue microarchitectural characteristics at dental implant sites. Part 1: identification of clinical-related parameters. *Clin Oral Implants Res* 23: 981-986
- Dias DR, Leles CR, Batista AC, Lindh C, Ribeiro-Rotta RF (2015) Agreement between Histomorphometry and Microcomputed Tomography to Assess Bone Microarchitecture of Dental Implant Sites. *Clin Implant Dent Relat Res* 17: 732-741
- Donos N, Retzepi M, Wall I, Hamlet S, Ivanovski S (2011) In vivo gene expression profile of guided bone regeneration associated with a microrough titanium surface. *Clin Oral Implants Res* 22: 390-398
- Farina R, Pramstraller M, Franceschetti G, Pramstraller C, Trombelli L (2011) Alveolar ridge dimensions in maxillary posterior sextants: a retrospective comparative study of dentate and edentulous sites using computerized tomography data. *Clin Oral Implants Res* 22: 1138-1144
- Gonzalez-Garcia R, Monje F (2013) Is micro-computed tomography reliable to determine the microstructure of the maxillary alveolar bone? *Clin Oral Implants Res* 24: 730-737
- Goto T, Nishinaka H, Kashiwabara T, Nagao K, Ichikawa T (2012) Main occluding area in partially edentulous patients: changes before and after implant treatment. *J Oral Rehabil* 39: 677-683
- Ibrahim N, Parsa A, Hassan B, van der Stelt P, Aartman IH, Wismeijer D (2014) Accuracy of trabecular bone microstructural measurement at planned dental implant sites using cone-beam CT datasets. *Clin Oral Implants Res* 25: 941-945
- Ilan N, Madri JA (2003) PECAM-1: old friend, new partners. *Curr Opin Cell Biol* 15: 515-24
- Kennedy E (1928) Partial denture construction. Dental Items of Interest Publishing Co, Brooklyn, NY
- Kopecka D, Simunek A, Brazda T, Rota M, Slezak R, Capek L (2012) Relationship between subsinus bone height and bone volume requirements for dental implants: a human radiographic study. *Int J Oral Maxillofac Implants* 27: 48-54
- Krings A, Rahman S, Huang S, Lu Y, Czernik PJ, Lecka-Czernik B (2012) Bone marrow fat has brown adipose tissue characteristics, which are attenuated with aging and diabetes. *Bone* 50: 546-552
- Lecka-Czernik B (2012) Marrow fat metabolism is linked to the systemic energy metabolism. *Bone* 50: 534-539

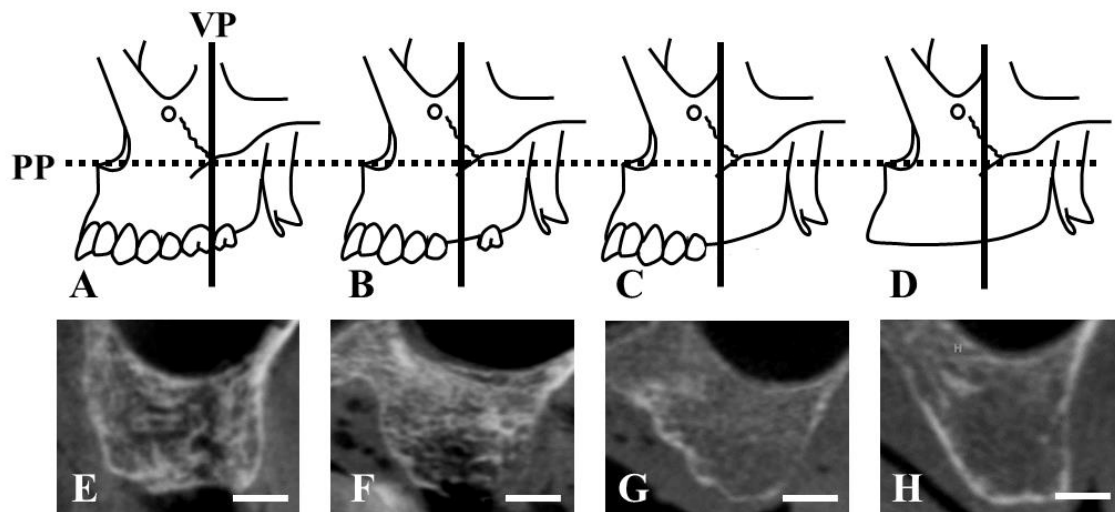
- Lee NK, Karsenty G (2008) Reciprocal regulation of bone and energy metabolism. *Trends Endocrinol Metab* 19: 161-166
- Marquezan M, Osorio A, Sant'Anna E, Souza MM, Maia L (2012) Does bone mineral density influence the primary stability of dental implants? A systematic review. *Clin Oral Implants Res* 23: 767-774
- Martinez H, Davarpanah M, Missika P, Celletti R, Lazzara R (2001) Optimal implant stabilization in low density bone. *Clin Oral Implants Res* 12: 423-432
- Misch CE (2015) Dental Implant Prosthetics, second edition. In: Misch CE Bone Density. Elsevier Health Sciences, St. Louis, Missouri: pp 237-252
- Monje A, Gonzalez-Garcia R, Monje F, Chan HL, Galindo-Moreno P, Suarez F, Wang HL (2015) Microarchitectural pattern of pristine maxillary bone. *Int J Oral Maxillofac Implants* 30: 125-132
- Monje A, Monje F, Gonzalez-Garcia R, Galindo-Moreno P, Rodriguez-Salvanes F, Wang HL (2014) Comparison between microcomputed tomography and cone-beam computed tomography radiologic bone to assess atrophic posterior maxilla density and microarchitecture. *Clin Oral Implants Res* 25: 723-728
- Muller R, van Campenhout H, van Damme B, van Der Perre G, Dequeker J, Hildebrand T, Rueggsegger P (1998) Morphometric analysis of human bone biopsies: a quantitative structural comparison of histological sections and micro-computed tomography. *Bone* 23: 59-66
- Muller R (2003) Bone microarchitecture assessment: current and future trends. *Osteoporos Int* 14 Suppl 5: S89-95; discussion S95-99
- Naitoh M, Hirukawa A, Katsumata A, Aiji E (2010) Prospective study to estimate mandibular cancellous bone density using large-volume cone-beam computed tomography. *Clin Oral Implants Res* 21: 1309-1313
- Naveiras O, Nardi V, Wenzel PL, Hauschka PV, Fahey F, Daley GQ (2009) Bone-marrow adipocytes as negative regulators of the haematopoietic microenvironment. *Nature* 460: 259-263
- NIH Consensus Development Panel (2001) Osteoporosis prevention, diagnosis, and therapy. *Jama* 285: 785-795

- Pabst AM, Walter C, Ehbauer S, Zwiener I, Ziebart T, Al-Nawas B, Klein MO (2015) Analysis of implant-failure predictors in the posterior maxilla: a retrospective study of 1395 implants. *J Craniomaxillofac Surg* 43: 414-420
- Parsa A, Ibrahim N, Hassan B, Motroni A, van Der Stelt P, Wismeijer D (2012) Reliability of voxel gray values in cone beam computed tomography for preoperative implant planning assessment. *Int J Oral Maxillofac Implants* 27: 1438-1442
- Parsa A, Ibrahim N, Hassan B, van Der Stelt P, Wismeijer D (2015) Bone quality evaluation at dental implant site using multislice CT, micro-CT, and cone beam CT. *Clin Oral Implants Res* 26: e1-7
- Pramstraller M, Farina R, Franceschetti G, Pramstraller C, Trombelli L (2011) Ridge dimensions of the edentulous posterior maxilla: a retrospective analysis of a cohort of 127 patients using computerized tomography data. *Clin Oral Implants Res* 22: 54-61
- Pusztaszeri MP, Seelentag W, Bosman FT (2006) Immunohistochemical expression of endothelial markers CD31, CD34, von Willebrand factor, and Fli-1 in normal human tissues. *J Histochem Cytochem* 54: 385-95
- Rasband WS, ImageJ, U. S. National Institutes of Health, Bethesda, Maryland, USA, <http://imagej.nih.gov/ij/>: 1997-2015
- Razavi R, Zena RB, Khan Z, Gould AR (1995) Anatomic site evaluation of edentulous maxillae for dental implant placement. *J Prosthodont* 4: 90-94
- Scardina GA, Pisano T, Messina M, Rallo A, Messina P (2011) "In vivo" evaluation of the vascular pattern in oral peri-implant tissues. *Arch Oral Biol* 56: 148-152
- Schropp L, Wenzel A, Kostopoulos L, Karring T (2003) Bone healing and soft tissue contour changes following single-tooth extraction: a clinical and radiographic 12-month prospective study. *Int J Periodontics Restorative Dent* 23: 313-323
- Sharan A, Madjar D (2008) Maxillary sinus pneumatization following extractions: a radiographic study. *Int J Oral Maxillofac Implants* 23: 48-56
- Trisi P, Rao W (1999) Bone classification: clinical-histomorphometric comparison. *Clin Oral Implants Res* 10: 1-7

- Ulm C, Kneissel M, Schedle A et al (1999) Characteristic features of trabecular bone in edentulous maxillae. *Clin Oral Implants Res* 10: 459-467
- Wang C, Meng H, Wang X, Zhao C, Peng J, Wang Y (2016) Differentiation of Bone Marrow Mesenchymal Stem Cells in Osteoblasts and Adipocytes and its Role in Treatment of Osteoporosis. *Med Sci Monit* 22: 226-233
- White SC, Pharoah MJ (2014) Oral Radiology: Principles and Interpretation, seventh edition. In: White SC Cone-Beam Computed Tomography. Elsevier Health Sciences, St. Louis, Missouri: pp 185-213
- Wirth AJ, Goldhahn J, Flaig C, Arbenz P, Muller R, van Lenthe GH (2011) Implant stability is affected by local bone microstructural quality. *Bone* 49: 473-478

Figure Legends

Fig. 1 CBCT image of the four forms in human maxilla



Schema of four forms of the maxillary first molar region based on the modified version of Kennedy's Classification: A, first molar dentulous; B, intermediately edentulous; C, partially edentulous; and D, fully edentulous (Kennedy 1928). Frontal view cross-sectional images were acquired for the four forms (E-H) (E, male, 80 years old; F, male, 80 years old; G, female, 79 years old; H, female, 97 years old). VP, vertical line at a right angle to the palatal plane (solid line); PP, horizontal line parallel to the palatal plane (dotted line) (Bar=5 mm).

Fig. 2 Bone density and structure in the four forms in human maxilla

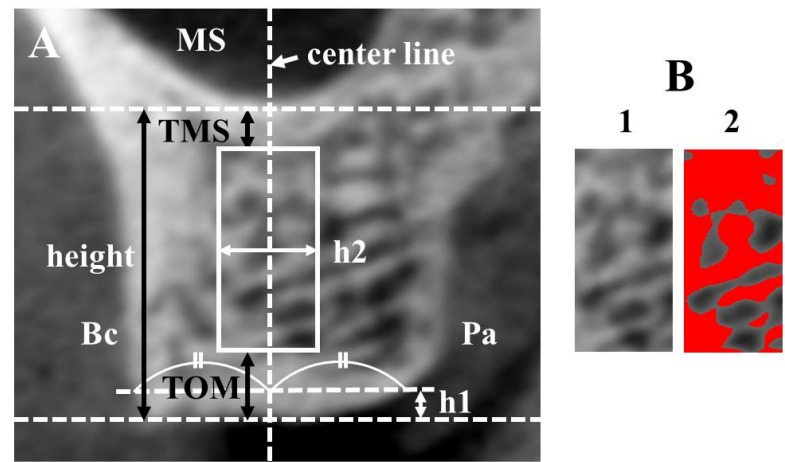
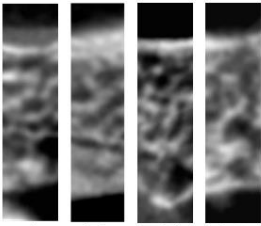
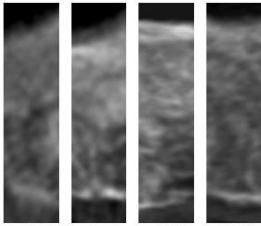
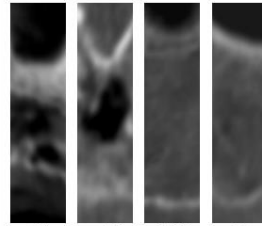


Fig. 2A shows a measurement point on a CBCT image. The center line is defined 1.5 mm (h1) above the tip of the maximum alveolar crest. Height was defined as the minimum bone border of the maxillary sinus side and the bone border of the oral mucosa side at the center line. Lines defining the thickness of the cortical bone at the maxillary sinus side (TMS) and the cortical bone at the oral mucosa side (OM) are shown. In Fig. 2B, the examined area includes a horizontal length of 4 mm (h2) (both line 2 mm in width from the center line). Images of cancellous bone (white square area, see Fig. 2A), as analyzed using Image J 1.48 software, are shown. The bone density of the cancellous bone was calculated using the ratio of an area of more than 200 mg/cm³ of HA. Bc, buccal side; MS, maxillary sinus; Pa, palatal side, B1, CBCT image; B2, modified software image.

Fig. 3 Classification of cancellous bone in human maxilla

	S 1	S 2	S 3
CaB	coarse	fine	IM, LIS
CBCT images	 A B C D	 E F G H	 I J K L

Cancellous bone structure was classified using the modified version of the Lekholm and Zarb classification. Cancellous bone (CaB) was classified into three bone structure categories: coarse (Type S1) (A, first molar dentulous (FMD), female, 73 years old; B, FMD, male, 72 years old; C, FMD, male, 64 years old; and D, FMD, male, 80 years old); fine (Type S2) (E, partially edentulous, male (PE), 77 years old; F, fully edentulous (FE), male, 78 years old; G, FE, male, 84 years old; and H, FE, male, 73 years old); and very soft bone with few incomplete mineralized trabecular bones (IM) and large intertrabecular spaces (LIS) (Type S3) (I, PE, female, 89 years old; J, FE, female, 86 years old; K, FE, female, 96 years old; and L, FE, male, 92 years old).

Fig. 4 Bone structure in the examined human maxilla

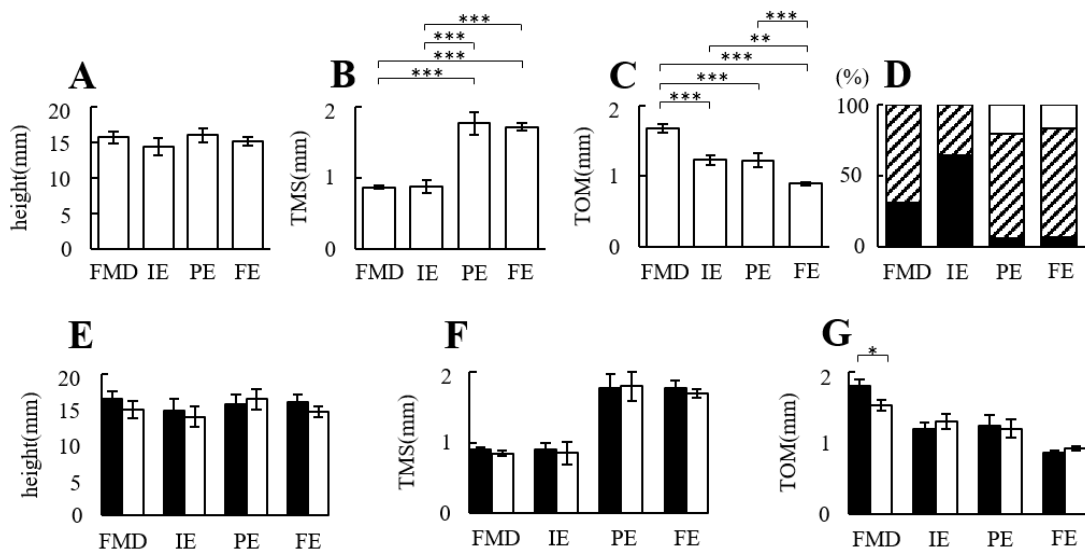


Fig. 4A, height of the maxillary bone (see Fig. 2A); Fig. 4B, TMS (see Fig. 2A); Fig. 4C, OM (see Fig. 2A); Fig. 4D, classification of cancellous bone structure (D, coarse (Type S1): black zone; fine (Type S2): slanted; IM and LIS (Type S3): white zone) (see Fig. 3); Fig. 4E, gender difference in the of height of the maxillary bone; Fig. 4F, gender difference in TMS; and Fig. 4G, gender difference in OM (E-G, male: black zone; female: white zone). *: $p < 0.05$, **: $p < 0.01$, ***: $p < 0.001$.

Fig. 5 Bone density in the examined human maxilla

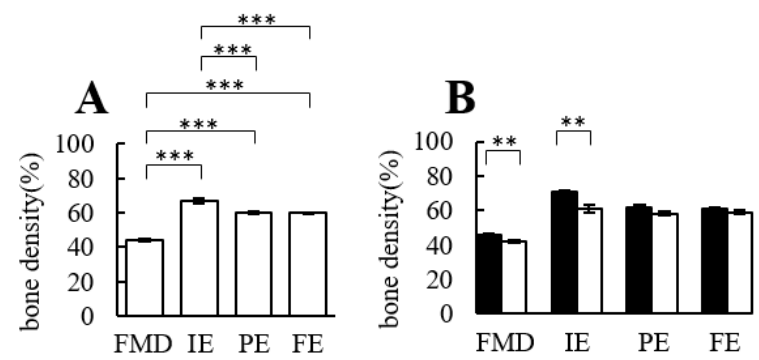
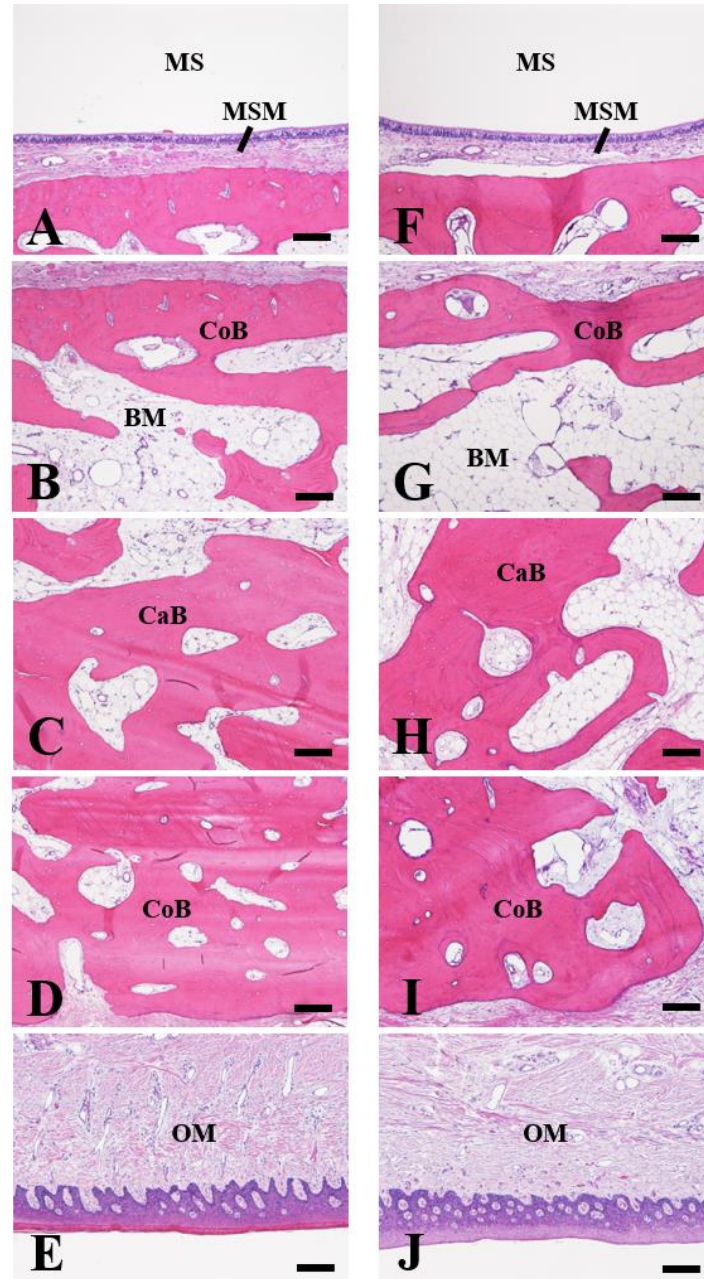


Fig. 5A, bone density of the maxillary bone (see Fig. 2C). Fig. 5B, gender difference in maxillary bone density (B, male: black zone; female: white zone). **: $p < 0.01$, ***: $p < 0.001$.

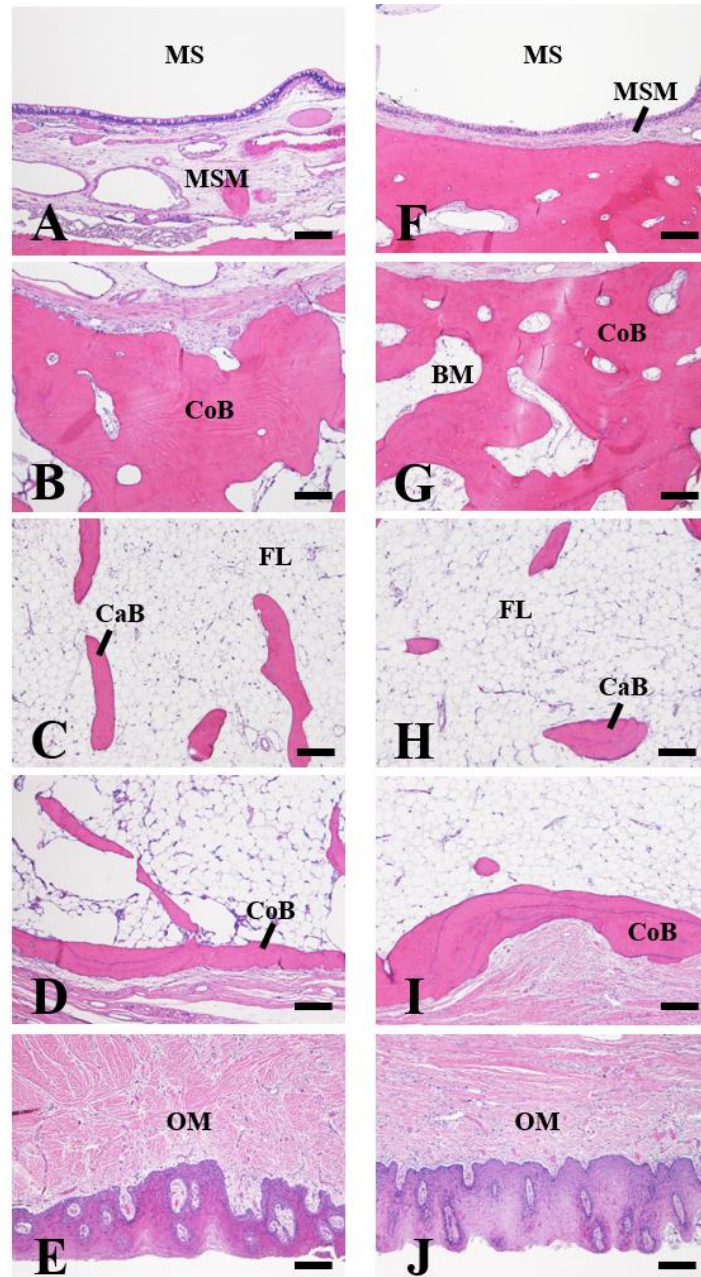
Fig. 6 Histochemical image (HE staining) of the first molar dentulous (FMD) and immediately edentulous (IE) human specimens



The maxillary sinus (MS) mucosa (MSM), oral mucosa (OM), and cortical bone (CoB) specimens are of almost the same thickness in FMD and IE (Figs. 6A and F). Moreover, the CoB structure is also identical between FMD and IE (Figs. 6B and G). Few fatty-like cells were observed in the bone marrow (BM) of FMD (Fig. 6C). Various forms including small and large bone marrow pockets were scattered in the CoB and cancellous bone (CaB) in both regions (Figs. 6C, D, H and I).

Figs. 6A and F show the MS side layer; Figs. 6B and G show the CoB (MS side); Figs. 6C and H show the CaB; Figs. 6D and I show the CoB (OM side); Figs. 6E and J show the OM side layer, Figs. 6A-E: FMD; Figs. 6F-J: IE (Bar=200 μ m).

Fig. 7 Histochemical image (HE staining) of the partially edentulous (PE) and the fully edentulous (FE) human specimens

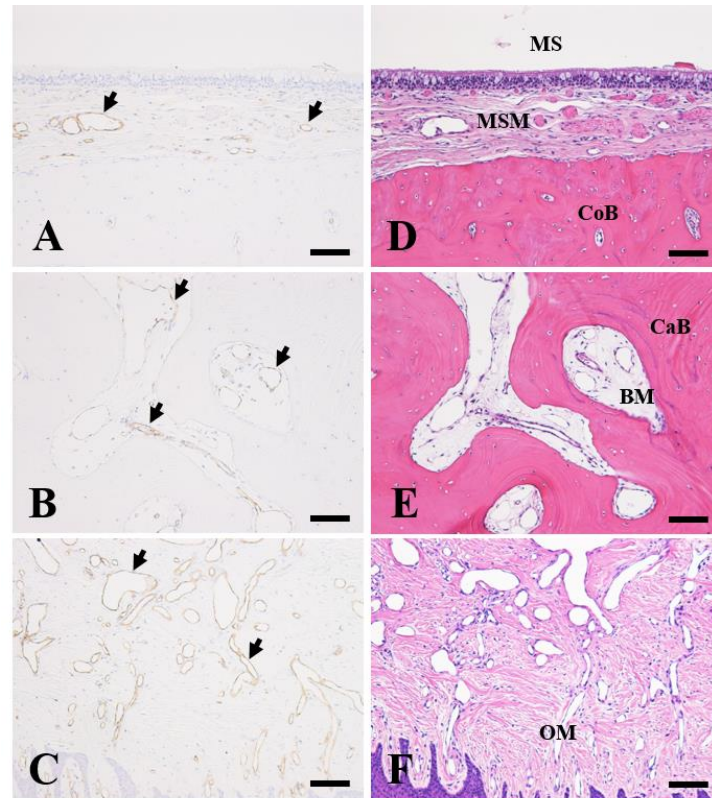


The maxillary sinus (MS) mucosa (MSM) layer including large vessels of the PE specimen is thicker

that of the FE specimen (Figs. 7A and F). The cortical bone (CoB) layer of MS side has thick, variously small and large bone marrow pockets in PE and FE (Figs. 7B and G), unlike that of the FMD and IE (Figs. 6B and G). Moreover, the cancellous bone (CaB) includes small and thin trabecular bones, which were scattered in the CaB (Figs. 7C, D, H and I). The cortical bone (CoB) layer of MS side has thin (Figs. 7D and me). The oral mucosa (OM) with epithelial layers of different thickness is found in the PE and FE (Figs. 7E and J) and is unlike the FMD and IE (Figs. 6E and J).

Figs. 7A and F show the MS side layer; Figs. 7B and G show the CoB (MS side); Figs. 7C and H show the CaB; Figs. 7D and I show the CoB (OM side); Figs. 7E and J show the OM side layer, Figs. 7A-E: PE; Figs. 7F-J: FE; BM, bone marrow; FL, fatty layer (Bar=200 μ m).

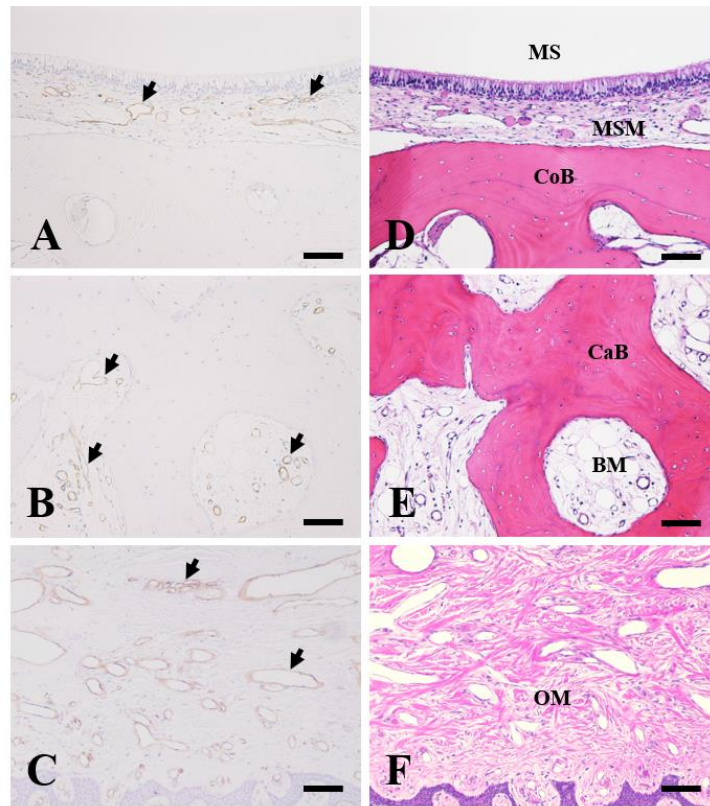
Fig. 8 Immunohistochemical staining using anti-CD31 and HE staining of serial sections in the first molar dentulous (FMD) human specimen



CD31-positive small ($< 50 \mu\text{m}\phi$) and intermediate (approximately $100 \mu\text{m}\phi$) vessels (arrows) were found in the connective tissue of the maxillary sinus (MS) mucosa (MSM) side (Figs. 8A and D). Small vessels were found in the bone marrow (BM) of the cortical bone (CoB) (Figs. 8A and D). In the cancellous bone

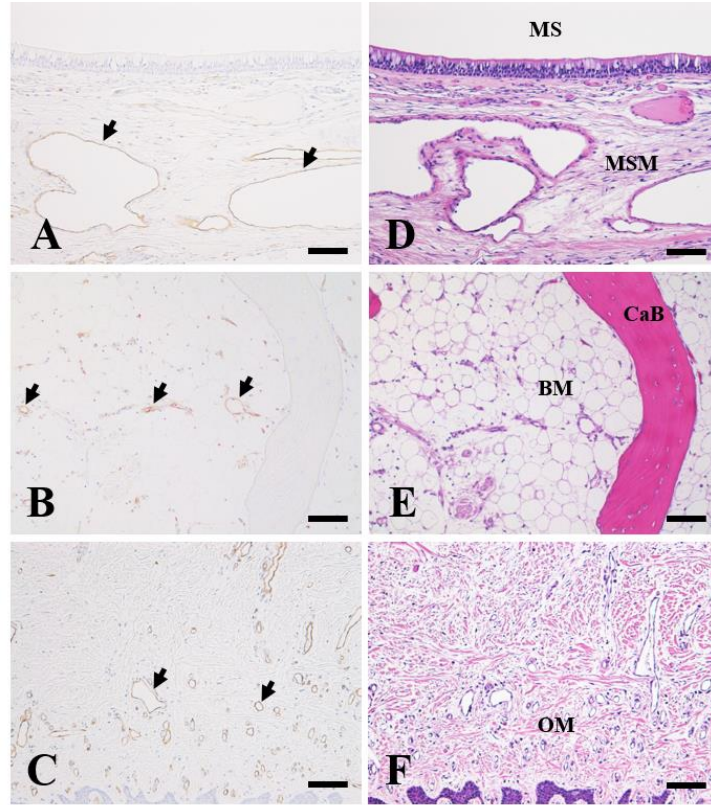
(CaB), various CD31-positive small and large ($>300\text{ }\mu\text{m}$) vessels (arrows) were observed in the BM (Figs. 8B and E). Numerous small oval and large elongated vessels (arrows) were localized at the oral mucosa (OM) side of the connective tissue (Figs. 8C and F). A-C: anti-CD31 staining; D-F: HE staining (Bar= $100\text{ }\mu\text{m}$).

Fig. 9 Immunohistochemical staining using anti-CD31 and HE staining of serial sections in the immediately edentulous (IE) human specimen.



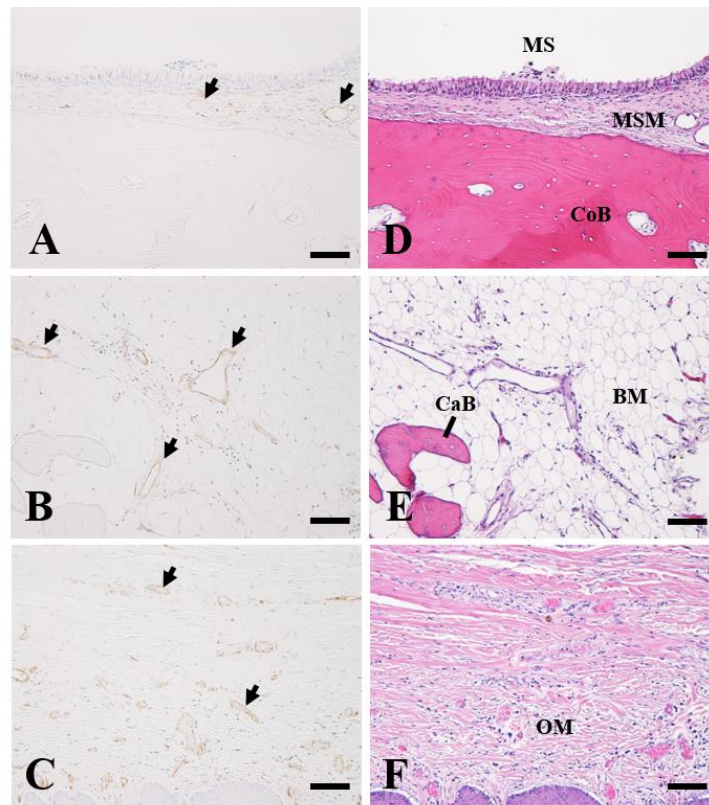
Small and intermediate CD31-positive vessels (arrows) were found in the connective tissue at the maxillary sinus (MS) mucosa (MSM) side (Figs. 9A and D). Small vessels were found in the bone marrow (BM) of the cortical bone (CoB) (Figs. 9A and D). Various CD31-positive small and large vessels (arrows) were found in the bone marrow of cancellous bone (CaB) (Figs. 9B and E). Moreover, numerous small and elongated CD31-positive vessels (arrows) were localized at the oral mucosa (OM) side of the connective tissue (Figs. 9C and F). A-C: anti-CD31 staining; D-F: HE staining (Bar= $100\text{ }\mu\text{m}$).

Fig. 10 Immunohistochemical staining using anti-CD31 and HE staining of serial sections in the partially edentulous (PE) human specimen



Large elongated CD31-positive vessels (arrows) were found at the maxillary sinus (MS) mucosa (MSM) side of the connective tissue (Figs. 10A and B). Small CD31-positive vessels (arrows) were found in the fatty bone marrow (BM) around elongated thin CaB (Figs. 10B and E). Moreover, small CD31-positive vessels (arrows) were localized at the oral mucosa (OM) side of the connective tissue (Figs. 10C and F). A-C: anti-CD31 staining; D-F: HE staining (Bar=100 μ m).

Fig. 11 Immunohistochemical staining using anti-CD31 and HE staining of serial sections in the fully edentulous human specimen



Small CD31-positive vessels (arrows) were found at the maxillary sinus (MS) mucosa (MSM) side of the connective tissue (Figs. 11A and B). Elongated small and large, CD31-positive vessels (arrows) were localized in the fatty bone marrow (BM) of small CaB (Figs. 11B and E). Small CD31-positive vessels (arrows) were scattered at the oral mucosa (OM) side of the connective tissue (Figs. 11C and F). A-C: anti-CD31 staining; D-F: HE staining (Bar=100 μ m).